Physica D 434 (2022) 133230

Contents lists available at ScienceDirect

Physica D

journal homepage: www.elsevier.com/locate/physd

Background-enhanced collapse instability of optical speckle beams in nonlocal nonlinear media

Gang Xu [a,b,*], Josselin Garnier [c], Adrien Fusaro [b,d], Antonio Picozzi [b]

[a] Dodd-Walls Centre, Physics Department, The University of Auckland, Private Bag 92019, Auckland 1142, New Zealand
[b] Laboratoire Interdisciplinaire Carnot de Bourgogne, CNRS, Université Bourgogne Franche-Comté, Dijon, France
[c] Centre de Mathematiques Appliquées, Ecole Polytechnique, 91128 Palaiseau Cedex, France
[d] CEA, DAM, DIF, F-91297 Arpajon Cedex, France

ARTICLE INFO

Article history:
Received 26 December 2021
Received in revised form 1 March 2022
Accepted 2 March 2022
Available online 9 March 2022

Keywords:
Nonlinear waves
Speckle beams
Collapse
Background
Optical turbulence

ABSTRACT

We study the focusing dynamics of incoherent wave-packets (speckle beams) in the presence of a nonlocal nonlinear response in the framework of the nonlocal nonlinear Schrödinger (NLS) equation. In the highly nonlocal regime, we show that the speckle beam develops a collective incoherent collapse instability — at variance with a conventional collapse that is inherently a coherent object, here it is the incoherent beam as a whole that develops a collapse. More specifically, we study the impact of a homogeneous incoherent background on the development of the incoherent collapse instability. Despite the fact that the homogeneous background is modulationally stable, we show that it significantly strengthens the formation of the incoherent collapse instability. Our theoretical analysis is based on a wave turbulence formulation of the Vlasov equation, which allows us to introduce an effective hydrodynamic model that is subsequently solved by the method of characteristics. A quantitative agreement is obtained between the simulations of the NLS equation, the Vlasov equation and the hydrodynamic model, without using adjustable parameters. The interaction between the background and the collapsing structure is described by means of a coupled system for the singular and smooth components of the solution of the Vlasov equation. The theory reveals that the mechanism underlying the background-induced collapse enhancement is due to a transfer of momentum from the background to the collapsing structure, while there is no 'mass' exchange among them. Furthermore, we show that a strong background level significantly boosts the collapse dynamics. Our work should stimulate the development of nonlinear experiments aimed at observing the incoherent collapse phenomenon in nonlinear thermal media. From a broader perspective, these investigations pave the way for the study of novel forms of global incoherent collective behaviors in wave turbulence, such as the formation of incoherent rogue waves.

1. Introduction

1.1. Weak turbulence, solitons and collapses

The wave turbulence theory provides a powerful tool to describe the nonequilibrium behavior of random dispersive nonlinear waves in the *weak nonlinear limit*. It has been successfully applied to various different contexts such as ocean waves, quantum fluids, plasmas, nonlinear optics [1–8], and more recently to gravitational waves [9,10]. However, the weak turbulence kinetic equation breaks down for *strong nonlinearities*, when the turbulent flow can be affected by strongly nonlinear excitations, e.g., collapsing wave-packets, rogue waves, vortices, (quasi-)solitons, or shock waves [2–8,11–18]. In this strongly nonlinear turbulent regime, a systematic theoretical approach is still missing [5].

A rather general physical mechanism responsible for the emergence of nonlinear coherent structures in a turbulent regime is provided by the inverse turbulence cascade, which carries 'mass' (power or wave-action) toward the low wave-number, i.e., toward the large scales. The inverse cascade increases the level of the nonlinearity up to a point where the weak turbulence description breaks down. In the defocusing regime, this nonlinear stage leads to a phenomenon of wave condensation [2,19–25]. On the other hand, in the focusing regime the homogeneous wave (condensate) is unstable and the Benjamin–Feir modulational instability leads to the formation of soliton-like states [4,7,12,

* Correspondence to: Wuhan National Laboratory for optoelectronics, School of Optical and Electronic Information, Huazhong University of Science and Technology, Wuhan 43007, China.
E-mail address: gang_xu@hust.edu.cn (G. Xu).

https://doi.org/10.1016/j.physd.2022.133230
0167-2789/

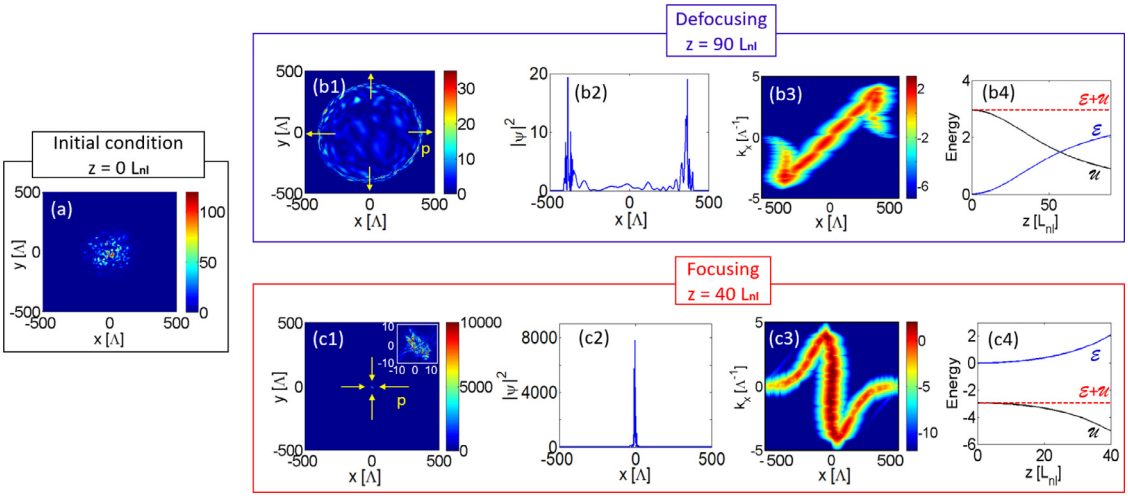

Fig. 1. Defocusing (annular singularity) vs. focusing (point singularity): Numerical simulations of the 2D NLS equation in the defocusing (upper) and focusing (lower) regimes. (a) Initial condition of the 2D speckle beam. Blue (red) frame shows the dynamics in the defocusing (focusing) regime at the propagation length $z = 90L_{nl}$ ($z = 40L_{nl}$). (b1,c1) report the 2D intensity distributions, while (b2,c2) report the corresponding lineouts at $y = 0$. The yellow arrows in (b1,c1) indicate the orientation of the momentum, which is radially ingoing (outgoing) in the focusing (defocusing) regime. (b3,c3) report the corresponding phase-space representation (or optical spectrogram). In the defocusing regime the random wave-packet exhibits an annular collapse singularity (the folding of the spectrogram takes place on the boundary of the beam), whereas in the focusing regime it exhibits a point collapse singularity (the folding of the spectrogram takes place at the beam center $x \simeq 0$). (b4,c4) report the evolutions of the linear contribution $\mathcal{E}(z)$ (blue line), and nonlinear contribution $\mathcal{U}(z)$ (black line), to the conserved Hamiltonian $\mathcal{H} = \mathcal{E} + \mathcal{U}$ (dashed red line). Note that in both the defocusing and focusing regimes, the singularity develops in the strongly nonlinear regime, with $\mathcal{E}(z = 0) \ll |\mathcal{U}(z = 0)|$. The collapse itself is *incoherent*, as evidenced by the broad spectral width at $x \sim 0$ in the spectrogram (c3) (see Eq. (19)), and the zoom over the 2D intensity distribution nearby $x \sim 0$ (see the inset in (c1)). The nonlocal range is $\sigma = 100\Lambda$.

26,27], or collapsing structures in relation with intermittency in turbulence [2,5,7,28].

It is important to recall that the nonlinear wave collapse has been widely studied for coherent waves. It refers to a strong contraction of the wave that leads to a catastrophic increase (blowup) of its amplitude after a finite time or a finite propagation distance. It has been observed in different branches of physics [29–32], including plasmas waves [33–35], Bose–Einstein condensates [36, 37], deep-water waves [38] and self focusing nonlinear optics [39–41]. It is worth-noting that collapse singularities also play a key role in astrophysics, where the gravitational attraction tends to compress stars above a critical mass leading to their collapse into neutron stars or even black holes [42]. The collapse dynamics has been widely discussed in the context of the nonlinear Schrödinger (NLS) equation, which is known as a universal model for dispersive nonlinear wave systems [29–32,43–46].

The collapse singularity signals a breakdown of the considered model equation: Nearby the singularity, the wave reaches an extreme high amplitude while the spatial and temporal scales get extremely small. However, the limit of validity of the model can be overcome by introducing different physical mechanisms. More specifically, the catastrophic collapse singularity can be regularized by introducing higher-order nonlinear effects describing the saturation of the nonlinearity [29], or higher-order dispersion effects describing non-paraxiality [47]. On the other hand, perturbative linear losses [30], and spatial incoherence [48–50], do not inhibit the collapse, while their effect is mainly to modify the blow-up threshold.

The nonlocal nature of the nonlinear interaction is another important physical effect that is known to arrest the collapse singularity [51–53]. A nonlocal wave interaction means that the response of the nonlinearity at a particular point is not determined solely by the wave intensity at that point, but also depends on the wave intensity in its neighborhood. Nonlocality thus constitutes a generic property of a large number of nonlinear wave systems [43,54–83].

1.2. Panoramic overview on different regimes

Our aim in this article is to investigate the collapse instability of random waves in the framework of the nonlocal NLS equation. In order to properly introduce our work, we start with a sort of panoramic overview over different relevant regimes. First of all, in order to favor the development of a collapse singularity, we consider the *strongly nonlinear regime* $\lambda_c^0 \gg \Lambda$, where λ_c^0 denotes the (initial) correlation length of the incoherent wave and Λ the healing length, i.e., the length scale such that linear and nonlinear effects are of the same order of magnitude [8]. In other terms, the strongly nonlinear regime means that the nonlinear contribution to the Hamiltonian dominates over the linear contribution, $|\mathcal{U}| \gg \mathcal{E}$, see Fig. 1 (see Section 2.1 for the definitions of $\mathcal{E}$ and $\mathcal{U}$.)

Let us now discuss the impact of the nonlocality by introducing the spatial range σ of the nonlocal interaction. If the nonlinear response is quasi-local $\sigma \lesssim \Lambda (\ll \lambda_c^0)$, the incoherent wave-packet develops several coherent collapses: Since the range of the nonlocal response is much smaller than the correlation length, each individual fluctuation (speckle) will undergo a collapse instability, which is, in a loose sense, almost independent of the collapse that occurs on a neighboring fluctuation. In other terms, in this quasi-local and strongly nonlinear regime, the speckle beam develops a series of *coherent* collapse singularities. This is in marked contrast with the highly nonlocal regime $\sigma \gg \lambda_c^0 \gg \Lambda$, where the incoherent wave-packet exhibits a collective behavior. This collective dynamics was analyzed in a previous work [68], where the propagation of a speckle beam was studied in the *defocusing* regime. Indeed, in the highly nonlocal defocusing regime, the speckle beam has been shown to exhibit a collective shock singularity. At variance with conventional shocks studied with coherent waves in local nonlinear media [84–95], here, the shock is termed 'collective' in the sense that it is the speckle beam as a whole that leads to the formation of the shock singularity, as illustrated in Fig. 1(b1)–(b2). In this defocusing regime, the fluctuations of the incoherent beam are 'pushed' toward the boundary of the beam, so that the front of the incoherent shock carries most of the stochastic fluctuations as well as most of

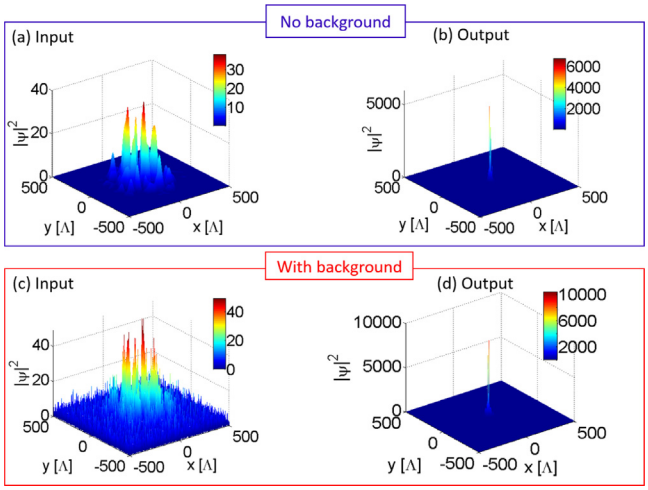

Fig. 2. Impact of an incoherent background on the collapse instability: Numerical simulations of the 2D NLS equation in the focusing regime showing the impact of an incoherent background. Initial speckle beam without background (a), and corresponding collapse peak formed at the propagation length $z = 68L_{nl}$ (b). (c) Same initial condition as in (a), but superimposed on a (modulationally stable) incoherent background, and corresponding collapse peak formed at the propagation length $z = 60L_{nl}$ (d). The presence of the incoherent background enhances the collapse peak amplitude (compare (b) and (d)).

the power (or 'mass'). As a consequence, the shock singularity is accompanied by the formation of an *annular collapse* singularity on the boundary of the beam, see Fig. 1(b1)–(b2). This double shock-collapse singularity is characterized by a specific folding of the spatial spectrogram (phase-space), as evidenced in Fig. 1(b3).

In the present paper, we consider the *focusing* regime of the highly nonlocal NLS equation. The physical picture for this regime is illustrated in the simulation reported in Fig. 1(c). At variance with the defocusing regime where the (average) momentum is radially out-going, in the focusing regime the momentum is inverted toward the center of the incoherent beam, see Fig. 1(c1)–(c2) where the arrows schematically indicate the orientation of the momentum $\mathbf{p}_{\rm NLS} \sim \Im(\psi^* \nabla \psi)$. As a result, the fluctuations are now 'pushed' toward the center of the beam, which thus exhibits a dramatic degradation of coherence (reduction of the coherence length). Indeed, as the system approaches the singular point, the spectral width increases dramatically at the beam center, a peculiar feature that is characterized by an inverted folding of the spectrogram, see Fig. 1(c3) nearby $x \simeq 0$. We stress again that the collapse is a collective incoherent phenomenon: At variance with the quasi-local regime where the individual fluctuations (speckles) of the incoherent beam exhibit a singularity almost independently of each other, here, it is the incoherent beam as a whole that exhibits a collective collapse singularity, i.e., the collapse is an incoherent object made of random waves. This aspect is evidenced in Fig. 1(c3) by the broad spectral width nearby the collapse point $x \simeq 0$. It is also evidenced by the 2D intensity distribution at the collapse point, which exhibits a speckle structure, see the zoom in the inset of Fig. 1(c1).

Our aim in this work is to characterize this collective incoherent collapse phenomenon. In particular, we study the impact of a *homogeneous incoherent background* on the incoherent collapse instability. It is important to note that we consider a regime where the *background itself is stable*, otherwise the incoherent modulation instability of the background becomes the main mechanism that affects the collapse behavior. A remarkable result of our theoretical analysis, which is confirmed by the numerical simulations, is that the *stable background favors* the development of the incoherent collapse instability. This is illustrated in the 2D-NLS simulation in Fig. 2. In Fig. 2(a)–(b) the incoherent beam develops the collapse singularity in the absence of the background. In Fig. 2(c)–(d) we consider exactly the same initial condition (same speckle beam with identical fluctuations), except that we superpose it on a homogeneous stable background. In this example, the ratio between the average background power and the average peak power of the speckle envelope is about 15%, which leads to a significant enhancement of the collapse peak, by a factor ∼2. In this work we will provide a more quantitative analysis of the impact of the background on the enhancement of the collapse peak instability through the analysis of different reduced effective models, see in particular Fig. 7. From a broader perspective, we remark that the impact of a background on the collapse instability has not been the subject of a systematic study. We note in particular that, at variance with the results reported here, in some specific regimes of the cubic-quintic NLS equation a coherent wave background has been shown to arrest the collapse instability [96]. On the other hand, in the case of the cubic NLS equation with long-range interactions ($\sigma \gg \Lambda$) considered in this work, the modulationally unstable coherent wave background can strengthen the development of the coherent collapse instability, as evidenced by numerical simulations.

In order to develop a theoretical analysis, we discuss in this article the mechanism of background-enhanced collapse instability in two different regimes, namely the weak background case (Section 3) and the strong background case (Section 4). Starting from the nonlocal NLS equation, our theory is based on a wave turbulence formulation of the long-range Vlasov equation (Section 2). The Vlasov equation is reduced to an effective hydrodynamic model for the singular collapse structure that is coupled to a reduced Vlasov-like equation describing the incoherent background. The analysis remarkably reveals that, in spite of the (modulational) stability of the homogeneous background, a transfer of momentum (instead of 'mass') takes place from the background toward the collapsing structure, which in turn leads to an enhancement of the collapse peak amplitude. We conclude in Section 5 by discussing the possible experimental verification of our theoretical predictions in nonlinear optics, by considering the propagation of speckle beams in thermal nonlinear media.

2. Theoretical modeling

2.1. Nonlocal NLS equation

A nonlocal nonlinearity is found in several systems, such as dipolar Bose–Einstein condensates [54], atomic vapors [43,55], nematic liquid crystals [7,58–60], glasses [61–64], thermal liquids [65–75], plasmas [76] and gravitational interactions [77–83]. We consider a general form of the nonlocal NLS equation in spatial dimension $d = 1$ or $d = 2$ describing the field propagation:

$$i\partial_z \psi = -\frac{\alpha}{2}\nabla_d^2 \psi - \gamma \psi \int U(\boldsymbol{r} - \boldsymbol{r}')\, |\psi|^2(\boldsymbol{r}', z)\, d\boldsymbol{r}', \tag{1}$$

where α denotes the diffraction parameter. Diffraction takes place in the transverse plane [$\boldsymbol{r} = x$ and $\nabla_1^2 = \partial_x^2$ for $d = 1$; $\boldsymbol{r} = (x, y)$ and $\nabla_2^2 = \partial_x^2 + \partial_y^2$ for $d = 2$], while the propagation axis z plays the role of an effective time variable. γ denotes the nonlinear coefficient and the interaction term includes an isotropic nonlocal response function [$U(\boldsymbol{r})$ that depends only on $r = |\boldsymbol{r}|$] with typical width σ denoting the range of the nonlocal interaction. We consider the focusing (attractive) nonlinear regime $\gamma > 0$. The healing length is defined by $\Lambda = \sqrt{\alpha L_{nl}}$, where $L_{nl} = 1/(\gamma\rho)$ is the nonlinear characteristic length, and $\rho = L^{-d}\int |\psi|^2 d\boldsymbol{r}$ the average intensity over the numerical window $[-L/2, L/2]^d$. We recall that the NLS Eq. (1) conserves two important quantities, the power $\mathcal{N} = \int |\psi(\boldsymbol{r}, z)|^2 d\boldsymbol{r}$ and the Hamiltonian $\mathcal{H} = \mathcal{E} + \mathcal{U}$, which

has a linear contribution $\mathcal{E}(z) = \alpha \int |\nabla\psi(\boldsymbol{r}, z)|^2 d\boldsymbol{r}$ and a nonlinear contribution $\mathcal{U}(z) = -\frac{\gamma}{2} \iint |\psi(\boldsymbol{r}, z)|^2 U(\boldsymbol{r}-\boldsymbol{r}')|\psi(\boldsymbol{r}', z)|^2 d\boldsymbol{r} d\boldsymbol{r}'$. As discussed in the previous section, we consider in this work initial conditions in the strongly nonlinear regime, so that $|\mathcal{U}| \gg \mathcal{E}$, see Fig. 1.

2.2. Wave turbulence Vlasov equation

The collapse-like behavior evidenced through the numerical simulations of the nonlocal NLS Eq. (1) in Figs. 1–2 refers to a single realization of the incoherent field $\psi(\boldsymbol{r}, z)$, which is inherently a stochastic function. To describe theoretically the collapse singularity, we need to resort to a deterministic description of the incoherent field that is based on an average over the realizations $\langle . \rangle$. Our theoretical description is developed in the general framework of the wave turbulence formalism. The wave turbulence theory has been shown to provide a natural asymptotic closure of the hierarchy of moment equations for a system of weakly nonlinear dispersive waves [1,3,5]. Here, the evolution of the incoherent wave-packet is characterized by fluctuations that are not homogeneous in space, so that, at leading order the dynamics is dominated by a long-range version of the Vlasov equation [8,68,97,98]. Note that the long-range Vlasov equation differs from the conventional Vlasov equation describing random waves (e.g., incoherent modulational instabilities, or incoherent solitons) in optics [8,99], hydrodynamics [12,18] or plasmas [100,101], while its structure is analogous to that describing systems of particles with long-range, e.g. gravitational, interactions [102]. In addition, at variance with conventional weak-turbulence approaches [1], the long-range Vlasov equation is valid beyond the weakly nonlinear regime of interaction [8,68,97,98,103,104]. We will see in the following that the long-range Vlasov Eq. (2) is found in quantitative agreement with the simulations of the NLS Eq. (1) in the strongly nonlinear regime.

We introduce the 'local' spectrum of the random wave that is defined as the Wigner-like transform of the correlation function

$$n_{\boldsymbol{k}}(\boldsymbol{r}, z) = \int B(\boldsymbol{r}, \boldsymbol{y}, z) \exp(-i\boldsymbol{k}\cdot\boldsymbol{y})\, d\boldsymbol{y},$$

with $B(\boldsymbol{r}, \boldsymbol{y}, z) = \langle \psi(\boldsymbol{r}+\boldsymbol{y}/2, z)\, \psi^*(\boldsymbol{r}-\boldsymbol{y}/2, z)\rangle$. As discussed above through Figs. 1–2, the spectrum is 'local' in the sense that it depends on the position $\boldsymbol{r}$, because the statistics of the random wave is not homogeneous in space. Starting from the nonlocal NLS Eq. (1) and considering the nonlocal regime of interaction $\sigma \gg \Lambda$, the local spectrum $n_{\boldsymbol{k}}(\boldsymbol{r}, z)$ can be shown to be governed by the long-range Vlasov equation [8]:

$$\partial_z n_{\boldsymbol{k}}(\boldsymbol{r}) + \partial_{\boldsymbol{k}}\Omega_{\boldsymbol{k}}(\boldsymbol{r}) \cdot \partial_{\boldsymbol{r}} n_{\boldsymbol{k}}(\boldsymbol{r}) - \partial_{\boldsymbol{r}}\Omega_{\boldsymbol{k}}(\boldsymbol{r}) \cdot \partial_{\boldsymbol{k}} n_{\boldsymbol{k}}(\boldsymbol{r}) = 0, \tag{2}$$

where $\Omega_{\boldsymbol{k}}(\boldsymbol{r}, z) = \omega(\boldsymbol{k}) + V(\boldsymbol{r}, z)$ is the generalized dispersion relation, with $\omega(\boldsymbol{k}) = \alpha|\boldsymbol{k}|^2/2$. Here, the effective potential reads

$$V(\boldsymbol{r}, z) = -\frac{\gamma}{(2\pi)^d} \int U(\boldsymbol{r}-\boldsymbol{r}') N(\boldsymbol{r}', z)\, d\boldsymbol{r}', \tag{3}$$

where $N(\boldsymbol{r}, z) = \int n_{\boldsymbol{k}}(\boldsymbol{r}, z) d\boldsymbol{k} = (2\pi)^d \left\langle |\psi(\boldsymbol{r}, z)|^2 \right\rangle$ denotes the average intensity. We recall that the Vlasov Eq. (2) conserves two important quantities, the total power ('mass') $\mathcal{N} = \int N(\boldsymbol{r}, z) d\boldsymbol{r}$ and the Hamiltonian $\mathcal{H} = \frac{1}{(2\pi)^d} \iint \omega(\boldsymbol{k}) n_{\boldsymbol{k}}(\boldsymbol{r}, z) d\boldsymbol{k} d\boldsymbol{r} + \frac{1}{2(2\pi)^d} \int V(\boldsymbol{r}, z) N(\boldsymbol{r}, z) d\boldsymbol{r}$.

We call the kinetic Eq. (2) 'wave turbulence Vlasov equation' to distinguish it from the conventional collisionless Boltzmann (Vlasov) equation in kinetic gas theory [105]. The Vlasov Eq. (2) describes the smooth evolution of the second-order moment $n_{\boldsymbol{k}}(\boldsymbol{r}, z)$ that is defined from the average over the realizations of the random wave, which differs from the spiky distribution solution of the collisionless Boltzmann kinetic equation.

The long-range Vlasov Eq. (2) describes a phenomenon of incoherent modulational instability. Incoherent modulational instability was originally described in the context of plasma physics [106]. More recently, incoherent modulational instability has been the subject of a detailed investigation in the optical context with an inertial response of the photorefractive nonlinearity [8,99,107,108]. A distinguished feature of incoherent modulational instability with respect to conventional modulational instability of a coherent wave is that it does not occur unconditionally for a focusing nonlinearity: The analysis reveals the existence of a damping term in the dispersion relation, which introduces a threshold for the incoherent modulational instability — the higher the degree of incoherence, the higher the value of the nonlinearity to exceed the threshold. Note that, the existence of a threshold for incoherent modulational instability was shown to be formally related to an effective Landau damping [109]. The modulational instability in the framework of the long-range Vlasov Eq. (2) is discussed in particular in Ref. [8]. As a consequence of the existence of a threshold, the incoherence of the waves can completely suppress the modulational instability. In the following and throughout the paper, we consider a homogeneous background that is *always modulationally stable*. In this way, the mechanism of background-enhanced collapse singularity discussed here is not due to the modulational instability of the background.

3. Impact of a weak background on the incoherent collapse

In this section we analyze both theoretically and numerically the impact of a weak background on the development of the incoherent collapse structure. Note that the Vlasov Eq. (2) describes the $2d$-dimensional phase-space $(\boldsymbol{r}, \boldsymbol{k})$ evolution of the random wave $\psi(\boldsymbol{x}, z)$ that evolves in d spatial dimensions. In order to perform accurate numerical simulations of the Vlasov Eq. (2) within a limited computational time, here we consider the purely one-dimensional case $d = 1$, while the extension to $d = 2$ will be considered later in Section 5.2.

3.1. Singular component coupled to a smooth component

In order to study the impact of the background on the collapsing structure, we split the general solution of the Vlasov Eq. (2) into a singular component $(N_S(x, z), K_S(x, z))$ and a smooth component describing the *modulationally stable* incoherent weak background, $m_k(x, z)$:

$$n_k(x, z) = N_S(x, z)\delta\big(k - K_S(x, z)\big) + m_k^{(1)}(x, z), \tag{4}$$

with

$$N_S(x, z) = N^{(0)}(x, z) + N^{(1)}(x, z), \tag{5}$$

$$K_S(x, z) = K^{(0)}(x, z) + K^{(1)}(x, z). \tag{6}$$

We note that the singular component with the Dirac $\delta-$function over the momentum finds its origin in the strongly nonlinear regime that is characterized by an extremely narrow spectral distribution. The singular solutions of the form of the first term on the right-hand side of Eq. (4) are also called 'mono-kinetic' [102], in the sense that each spatial position (x) corresponds to a unique spectral (velocity) component (k).

We assume that the homogeneous background is weak and thus $N^{(1)}(x, z)$, $K^{(1)}(x, z)$ and $m_k^{(1)}(x, z)$ are of higher order with respect to $N^{(0)}(x, z)$, $K^{(0)}(x, z)$. More precisely, we have $N(x, z) = \int n_k(x, z) dk = N_S(x, z) + M^{(1)}(x, z) = N^{(0)}(x, z) + N^{(1)}(x, z) + M^{(1)}(x, z)$ with $M^{(1)}(x, z) = \int m_k^{(1)}(x, z) dk$ and $N^{(0)}(x, z) \gg N^{(1)}(x, z), M^{(1)}(x, z)$. Then 'weak' background means that the average intensity of the background $M^{(1)}(x, z)$ is much smaller than that of the perturbation $N^{(0)}(x, z)$. The sign of $N^{(1)}(x)$ is important and denotes an enhancement or a decrease of the collapsing structure due to the presence of the stable background.

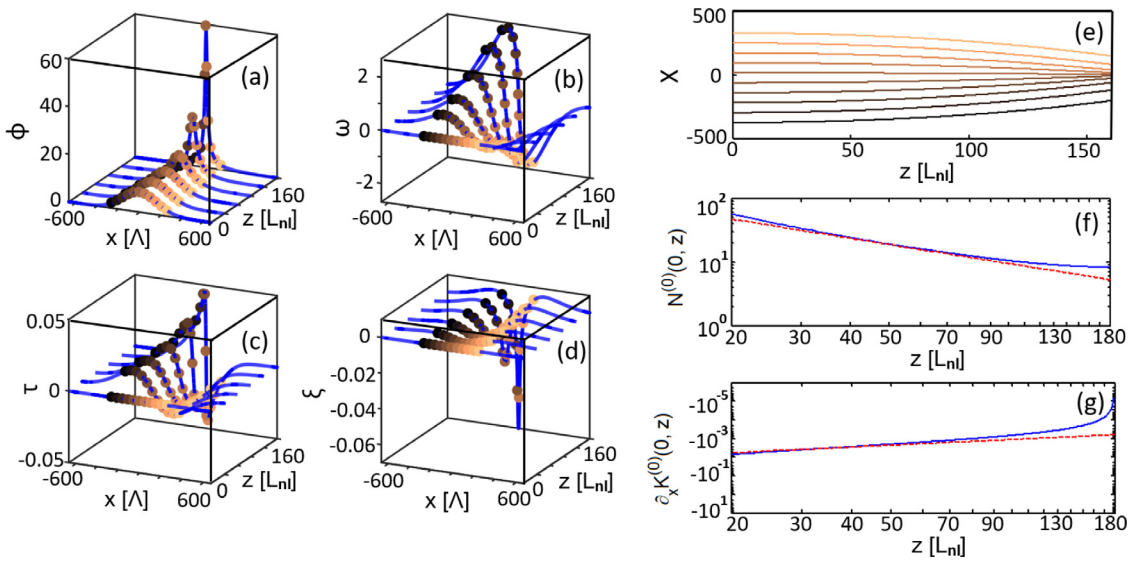

Fig. 3. Collapse dynamics without background: hydrodynamic and characteristic ODE simulations. Numerical simulations of the hydrodynamic model Eq. (7)–(9) (blue line), and of the coupled system of characteristics ODE Eqs. (10)–(14) (filled circles). Evolution of the intensity envelope $N^{(0)}(x,z)$ [or $\phi(z)$] (a), the momentum $K^{(0)}(x,z)$ [or $w(z)$] (b), the 'temporal' $z-$gradient of the momentum $\partial_z K^{(0)}(x,z)$ [or $\tau(z)$] (c), and the spatial $x-$gradient of the momentum $\partial_x K^{(0)}(x,z)$ [or $\xi(z)$] (d), for different characteristics $X(z)$ (e). The momentum $K^{(0)}(x,z)$ exhibits a shock singularity (b), i.e. a collapse singularity for the gradient $\partial_x K^{(0)}(x,z)$ (d), which in turn induces a collapse singularity for the intensity envelope $N^{(0)}(x,z)$ (a). Evolutions during the propagation of the intensity envelope $\phi(z)$ (f), and gradient of the momentum $\xi(z)$ (g), of the incoherent beam along the characteristic $X(z)=0$ (e). Their evolutions exhibit the power-law divergence $\sim(z_\infty - z)^{-1}$ predicted by the theory in Eqs. (17)–(18) (dashed red lines) ($\sigma = 200\Lambda$).

3.2. Collapse dynamics at the leading zero-th order: No background

We substitute the general form of the solution given in Eqs. (4)–(6) into the Vlasov Eq. (2). We obtain at zero-th order the following set of hydrodynamic-like equations for the evolutions of the density and momentum:

$$\partial_z N^{(0)} + \alpha \partial_x (N^{(0)} K^{(0)}) = 0, \tag{7}$$

$$\partial_z K^{(0)} + \alpha K^{(0)} \partial_x K^{(0)} + \partial_x V^{(0)} = 0, \tag{8}$$

$$V^{(0)}(x,z) = -\frac{\gamma}{2\pi} \int U(x-x') N^{(0)}(x',z) dx'. \tag{9}$$

This set of equations is closed and describes the evolution of the system at the leading order.

Starting from $K^{(0)}(x, z=0) = 0$, the momentum $K^{(0)}(x,z)$ is initially driven by the last nonlinear term in (8), while the Burgers-like (second) term of (8) subsequently leads to the gradient catastrophe of $K^{(0)}(x,z)$ toward the point $x=0$. The finite 'time' (distance, z) shock singularity of $K^{(0)}(x,z)$ is responsible for a collapse singularity of the intensity envelope $N^{(0)}(x=0,z)$. These singular behaviors can be described theoretically by solving the hyperbolic Eqs. (7)–(8) by the method of characteristics [110]. We define $w(z) = K^{(0)}(X(z),z)$, $\tau(z) = \partial_z K^{(0)}\big(X(z),z\big)$, $\xi(z) = \partial_x K^{(0)}\big(X(z),z\big)$, and $\phi(z) = N^{(0)}\big(X(z),z\big)$, which can be shown to satisfy a set of coupled ordinary differential equations (ODE):

$$\dot{X}(z) = \alpha w(z), \tag{10}$$

$$\dot{w}(z) = \tau(z) + \alpha w(z)\xi(z), \tag{11}$$

$$\dot{\tau}(z) = -\partial_{zx}^2 V^{(0)}(X(z),z) - \alpha \xi(z)\tau(z), \tag{12}$$

$$\dot{\xi}(z) = -\partial_x^2 V^{(0)}(X(z),z) - \alpha \xi^2(z), \tag{13}$$

$$\dot{\phi}(z) = -\alpha \xi(z)\phi(z). \tag{14}$$

In Eqs. (10)–(14), the dots denote the 'temporal' derivatives, $\dot{X}(z) = \partial_z X(z)$, and so on. For a given characteristic $X(0) = x_0$, the initial conditions are $w(0)=0$, $\tau(0) = -\partial_x V^{(0)}(x_0, z=0)$, $\xi(0) = 0$, $\phi(0) = N^{(0)}(x_0, z=0)$.

The collapse singularity of $N^{(0)}(x,z)$ occurs nearby $x=0$, then there exists some 'time' (distance, z) above which the width of $N^{(0)}(x,z)$ becomes much smaller than the range of the nonlocal nonlinearity, σ, so that the effective potential can be approximated by $V^{(0)}(x,z) \simeq -\gamma \mathcal{N}^{(0)} U(x)$, with $\mathcal{N}^{(0)} = (2\pi)^{-1} \int N^{(0)}(x,z)dx$. Note that, to study the behavior of the solution nearby $x \sim 0$, one can consider the characteristic with $x_0 = 0$. Then if $U(x)$ is smooth and maximal at $x=0$ (such as the Gaussian-shaped response function considered in the simulations), then $\partial_x U(0) = 0$, so that $\tau(z) = 0$, $w(z) = 0$, $X(z) = 0$ along this characteristic.

More generally, by defining $\kappa^2 = -\gamma \mathcal{N}^{(0)} \partial_x^2 U(0) > 0$, the solutions to Eqs. (13)–(14) read

$$\partial_x K^{(0)}(0,z) = -\frac{\kappa}{\sqrt{\alpha}} \tan(\sqrt{\alpha}\kappa z), \tag{15}$$

$$N^{(0)}(0,z) = \frac{N^{(0)}(0)}{\cos(\sqrt{\alpha}\kappa z)}. \tag{16}$$

This shows that the gradient of the spectrogram and the intensity exhibit a finite time collapse at $x=0$, with $z_\infty = \pi/(2\kappa)$. In particular, just before the singularity

$$\partial_x K^{(0)}(0,z) \simeq \frac{-1}{\alpha(z_\infty - z)}, \tag{17}$$

$$N^{(0)}(0,z) \simeq \frac{N^{(0)}(0)}{\sqrt{\alpha}\kappa(z_\infty - z)}. \tag{18}$$

We have performed numerical simulations of the hydrodynamic model Eqs. (7)–(8), and the complete set of characteristic ODE Eqs. (10)–(14), see Fig. 3. The evolutions of the characteristics $X(z)$ are reported in panel Fig. 3(e) for an ensemble of initial conditions $X(0) = x_0$, which evidence that the characteristics tend to converge nearby the shock point along the characteristic $X(z)=0$. The evolution of the momentum $w(z)$ of the incoherent beam for such a set of initial conditions exhibits a shock singularity, see Fig. 3(b). The gradient catastrophe is reflected by the evolution of $\xi(z)$ that exhibits a (negative) collapse singularity [see Fig. 3(d)], which in turn induces a collapse singularity of the intensity envelope $\phi(z)$ of the incoherent beam, see Fig. 3(a). We have also verified that $\phi(z)$ and $\xi(z)$ exhibit a finite time

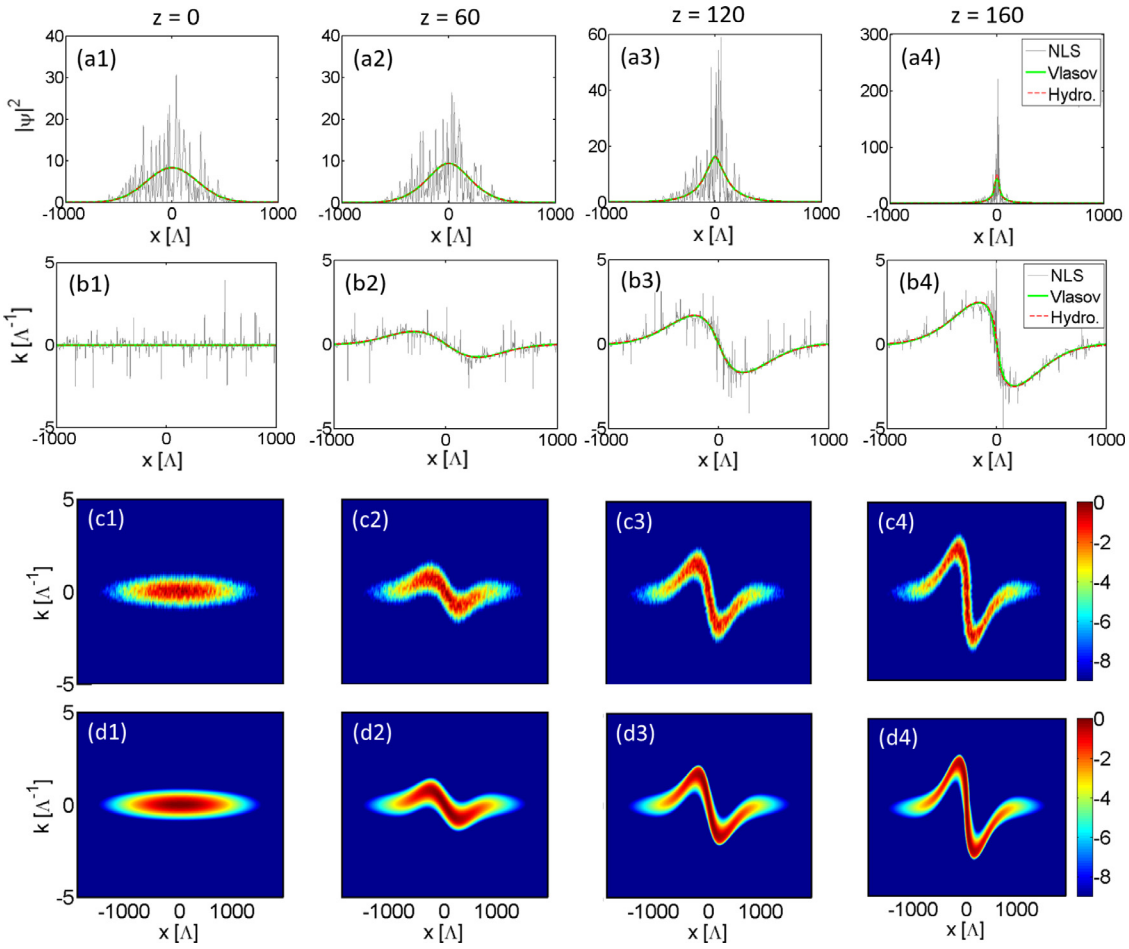

Fig. 4. Collapse dynamics without background: NLS, Vlasov and hydrodynamic simulations. (a)–(b) Numerical simulations of the NLS Eq. (1) (gray line), Vlasov Eq. (2) (green line) and hydrodynamic model Eqs. (7)–(8) (dashed red line), showing the evolutions during the propagation of the intensity (a), and the momentum (b), of the random field. The dashed-blue lines in (a) show the intensity envelopes of the initial wave-packets. (c) Corresponding phase-space evolution obtained from the NLS simulation. (d) Corresponding phase-space evolution obtained from the Vlasov simulation. The good agreement between the simulations of the NLS, Vlasov and hydrodynamic equations has been obtained *without using adjustable parameters*. Parameters are the same as in Fig. 3, $\sigma = 200\Lambda$, the initial incoherent beam has a Gaussian envelope.

singularity with the expected power-law divergence given by (17)–(18), as illustrated in Fig. 3(f)–(g).

In order to test the validity of the theory within the original model equations, we have also performed simulations of the NLS Eq. (1) and the Vlasov Eq. (2). We report in Fig. 4 the simulation of the NLS equation starting from a spatially localized random wave with Gaussian envelope, and the corresponding Vlasov simulation. As discussed in the introduction section, the initial condition is strongly nonlinear $\mathcal{E}(z=0) \ll |\mathcal{U}(z=0)|$ with $\mathcal{H} = \mathcal{E} + \mathcal{U} < 0$ (see Fig. 1(c4)), or $\lambda_c^0 \gg \Lambda$. The corresponding phase-space (x, k) evolution of the fields is also reported in Fig. 4, which evidences the excellent agreement that is obtained between the simulations of the NLS Eq. (1) and Vlasov Eq. (2) without using adjustable parameters, see panels (c) and (d) in Fig. 4. The peculiar folding of the phase-space spectrogram is characterized by a significant local increase of the spectral width nearby the collapse point at $x \simeq 0$ and $z \simeq 160 L_{nl}$. Note that the spectral width at the collapse point is of the order

$$\Delta k_\infty \simeq 2\pi/\lambda_c^\infty \simeq 2\pi/\Lambda, \tag{19}$$

see panels (c4) and (d4) in Fig. 4. This means that the singularity is regularized when the correlation length becomes of the order of the healing length, $\lambda_c^\infty \sim \Lambda$. Nearby the collapse point, the field intensity exhibits a large incoherent peak at $x \sim 0$, with peak power about $\sim$ 10 times larger than the peak intensity of the initial Gaussian envelope (denoted by the blue line in Fig. 4(a)). Note that, as discussed here above through the characteristic Eqs. (10)–(14), the hydrodynamic model Eqs. (7)–(8) exhibits a finite 'time' singularity, so that the model breaks down nearby the collapse point $z \lesssim z_\infty$, while the singularity is regularized in the NLS and Vlasov equations by higher-order terms neglected in the hydrodynamic model Eqs. (7)–(8).

3.3. Dynamics at the first-order: Impact of the weak background

Let us now study the impact of a weak background on the collapse dynamics. For this purpose, we consider the perturbation expansion at the next first-order. By substitution of the expansion given in Eqs. (4), (5), (6), we obtain the following set of equations:

$$\partial_z N^{(1)} + \alpha \partial_x (N^{(0)} K^{(1)} + N^{(1)} K^{(0)}) = 0, \tag{20}$$

$$\partial_z K^{(1)} + \alpha \partial_x (K^{(0)} K^{(1)}) + \partial_x (V^{(1)} + V_M^{(1)}) = 0, \tag{21}$$

$$\partial_z m_k^{(1)} + \alpha k \partial_x m_k^{(1)} - \partial_x V^{(0)} \partial_k m_k^{(1)} = 0, \tag{22}$$

with

$$V^{(1)}(x,z) = -\frac{\gamma}{2\pi} \int U(x-x') N^{(1)}(x',z) dx', \tag{23}$$

$$V_M^{(1)}(x,z) = -\frac{\gamma}{2\pi} \int U(x-x') M^{(1)}(x',z) dx'. \tag{24}$$

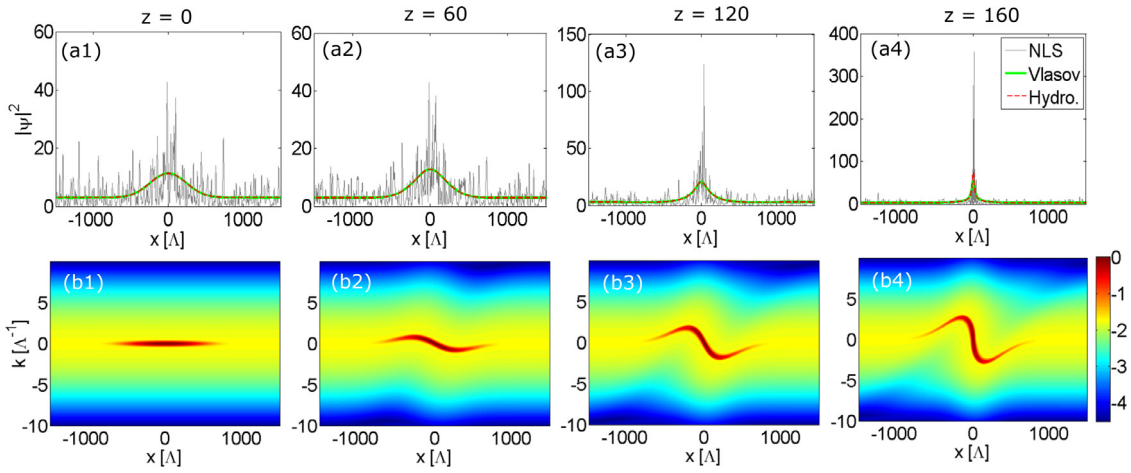

Fig. 5. Collapse dynamics with weak background: NLS, Vlasov and hydrodynamic simulations. (a) Numerical simulations of the NLS Eq. (1) (gray line), Vlasov Eq. (2) (green line) and hydrodynamic equations (dashed red line). The hydrodynamic model consists of the zero-order contribution $(N^{(0)}(x,z), K^{(0)}(x,z))$ given by Eqs. (7)–(8), and the first-order contribution $(N^{(1)}(x,z), K^{(1)}(x,z))$ given by Eqs. (20)–(21) that is coupled to the incoherent background $m_k^{(1)}(x,z)$ governed by the reduced Vlasov Eq. (22): The dashed red line reports $N(x,z) = N^{(0)}(x,z) + N^{(1)}(x,z) + M^{(1)}(x,z)$. (b) Corresponding phase-space evolution obtained from the simulation of the Vlasov Eq. (2). The parameters are the same as in Fig. 4, except that a modulationally stable weak background has been added. The good agreement between the simulations of the NLS, Vlasov and hydrodynamic equations has been obtained without using adjustable parameters. The nonlocal range is $\sigma = 200\Lambda$.

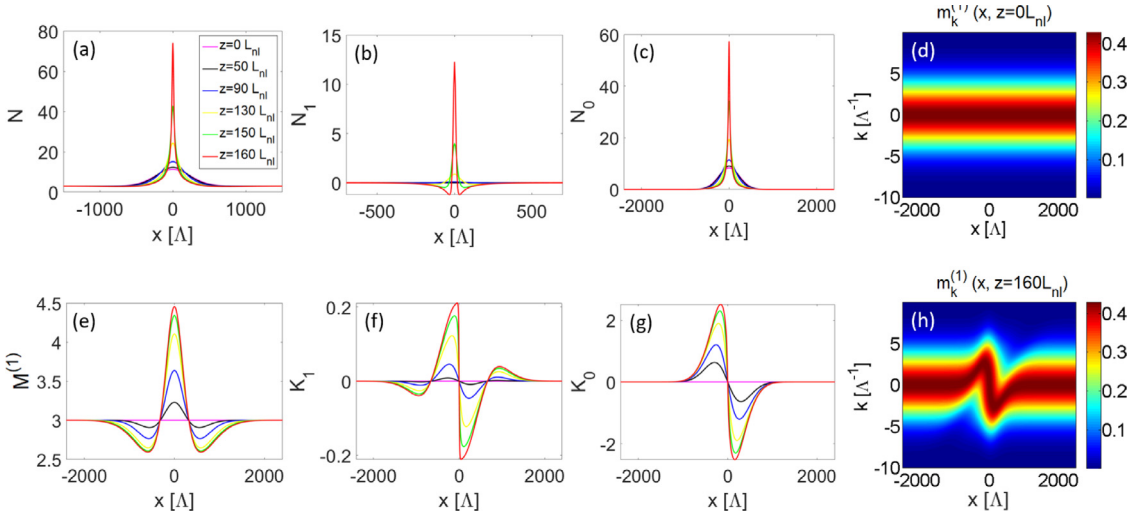

Fig. 6. Collapse dynamics with weak background: Detailed hydrodynamic simulations. Numerical simulation of the complete hydrodynamic model, which includes the zero-order contribution $(N^{(0)}(x,z), K^{(0)}(x,z))$ given by Eqs. (7)–(8) (in (c) and (g)), the first-order contribution $(N^{(1)}(x,z), K^{(1)}(x,z))$ given by Eqs. (20)–(21) (in (b) and (f)) and its coupling to the incoherent background $m_k^{(1)}(x,z)$ governed by the reduced Vlasov Eq. (22) (in (d) and (h)), with the intensity $M^{(1)}(x,z) = \int m_k^{(1)}(x,z)dk$ (in (e)). The sum of the intensity contributions $N(x,z) = N^{(0)}(x,z) + N^{(1)}(x,z) + M^{(1)}(x,z)$ is reported in (a). The different colors report the quantities at different propagation lengths, see the legend in (a). The transfer of momentum $K^{(1)}(x,z)$ between the background and the collapse structure drives the background-enhanced collapse: The sign of $N^{(1)}(x)$ is important and denotes an enhancement ($N^{(1)}(x) > 0$) or a decrease ($N^{(1)}(x) < 0$) of the collapsing structure due to the presence of the stable background. The 'mass' on both sides of the localized beam $N^{(1)}(x,z)$ is transferred toward the beam center, which leads to an enhancement of the collapse structure at $x \simeq 0$. We recall that there is no 'mass' exchange between the background and the collapse structure ($\int N^{(1)}(x,z)dx = 0$ for any z). Parameters are the same as in Fig. 5.

The initial conditions verify $K^{(0)}(x, t = 0) = K^{(1)}(x, t = 0) = N^{(1)}(x, t = 0) = 0$. Note that, if there is no background, $m_k^{(1)}(x,z) = 0$, then $V_M^{(1)}(x,z) = 0$, so that $N^{(1)}$ does not grow: $N^{(1)}(x,z) = 0$ throughout the evolution, i.e., we recover the leading zero-order evolution described by Eqs. (7)–(8).

The following quantities are conserved during the evolution in z: $\mathcal{N}^{(0)} = (2\pi)^{-1}\int N^{(0)}(x,z)dx$, $\mathcal{N}^{(1)} = (2\pi)^{-1}\int N^{(1)}(x,z)dx$, $\mathcal{M}^{(1)} = (2\pi)^{-1}\int M^{(1)}(x,z)dx$. This means that the collapse enhancement mediated by the background, is not due to a transfer of 'mass' (power) from the background toward the collapsing structure. It is due to a transfer of momentum from the background toward the singular component: the last term $\partial_x V_M^{(1)}$ in Eq. (21) originates in the background and it induces a local growth of the momentum $K^{(1)}$. In turn, this induces a growth of $N^{(1)}$ nearby the singular point ($x \simeq 0, z \lesssim z_\infty$), which leads to an enhancement of the collapse structure.

This key mechanism of background-enhanced collapse instability is evidenced by the numerical simulations of the hydrodynamic Eqs. (20)–(21) for $(N^{(1)}, K^{(1)})$ coupled to the Vlasov-like Eq. (22) for the incoherent background $m_k^{(1)}(x,z)$. The results of the simulation are reported in Figs. 5–6. Aside from the good agreement between the NLS Eq. (1) and Vlasov Eq. (2), we also note the good agreement with the hydrodynamic model. This latter model includes the leading zero-order contribution $(N^{(0)}, K^{(0)})$ [Eqs. (7)–(8)], the first-order contribution [Eqs. (20)–(21)] and its coupling to the incoherent background $m_k^{(1)}(x,z)$ ruled by the Vlasov-like Eq. (22). The dashed red line in Fig. 5(a) reports $N(x,z) = N^{(0)}(x,z) + N^{(1)}(x,z) + M^{(1)}(x,z)$ (with $M^{(1)}(x,z) =$

$\int m_k^{(1)}(x,z)dk$), which is in quantitative agreement with the simulation of the original Vlasov Eq. (2).

As commented above, there is no transfer of 'mass' (power) from the background to the collapsing structure since $\mathcal{N}^{(0)}$, $\mathcal{N}^{(1)}$ and $\mathcal{M}^{(1)}$ are conserved. However, we clearly see in Fig. 6(b) that the initial homogeneous profile of $N^{(1)}(x)$ is modified in such a way that the 'mass' on both sides of the localized beam is transferred toward the beam center, which leads to a reinforcement of the collapse peak at $x = 0$. The peculiar deformation of $N^{(1)}$ is due to a transfer of momentum from the incoherent background to the collapse structure, as evidenced by the evolution of $K_1(x,z)$ in Fig. 6(f). As discussed above, such a transfer of momentum is driven by the last term in Eq. (22). Notice that the peculiar deformation of $N^{(1)}$ is also observed in the evolution of the incoherent background intensity $M^{(1)}(x,z)$, as shown in Fig. 6(d)–(h).

4. Impact of a strong background on the incoherent collapse

In the previous section, we have shown that a *weak* homogeneous incoherent background enhances the development of the incoherent collapse instability. However, since the background is of small amplitude, its impact on the collapse dynamics is moderate. In this section we study the impact of a *strong* homogeneous incoherent background. As we will see, such a strong background significantly boosts the collapse dynamics, despite the fact that the background is modulationally stable.

4.1. Singular component coupled to a smooth component

In order to study the impact of a strong background on the collapsing structure, we need to modify the approach discussed in Section 3. In the case of a strong background, the leading order solution is the stable homogeneous background $m_k^{(0)}$. We split the general solution of the Vlasov equation into a singular component and a smooth component describing the strong background $m_k^{(0)}$ and its perturbation $m_k^{(1)}(x,z)$:

$$n_k(x,z) = N^{(1)}(x,z)\delta\big(k - K^{(1)}(x,z)\big) + m_k(x,z), \tag{25}$$

with

$$m_k(x,z) = m_k^{(0)} + m_k^{(1)}(x,z). \tag{26}$$

Accordingly, we have $N(x,z) = \int n_k(x,z)dk = N^{(1)}(x,z) + M^{(0)} + M^{(1)}(x,z)$ with $M^{(0)} = \int m_k^{(0)}dk$, $M^{(1)}(x,z) = \int m_k^{(1)}(x,z)dk$, and $M^{(0)} \gg M^{(1)}(x,z), N^{(1)}(x,z)$. Then 'strong' background means that the average intensity of the background $M^{(0)}$ is much larger than that of the perturbation $N^{(1)}(x,z)$. The sign of $M^{(1)}(x)$ is important, it denotes an enhancement or a decrease of the collapsing structure due to the presence of the stable background.

By substitution of (25)–(26) into the Vlasov Eq. (2), the different components satisfy

$$\partial_z m_k^{(1)} + \alpha k \partial_x m_k^{(1)} - \partial_x V^{(1)} \partial_k m_k^{(0)} = 0, \tag{27}$$

$$\partial_z N^{(1)} + \alpha \partial_x (N^{(1)} K^{(1)}) = 0, \tag{28}$$

$$\partial_z K^{(1)} + \alpha K^{(1)} \partial_x K^{(1)} + \partial_x V^{(1)} = 0, \tag{29}$$

starting from $N^{(1)}(x, z = 0) = N_o^{(1)}(x)$, $m_k^{(1)}(x, z = 0) = 0$, $K^{(1)}(x, z = 0) = 0$, with

$$V^{(1)}(x,z) = -\frac{\gamma}{2\pi}\int U(x-x')[N^{(1)} + M^{(1)}](x',z)dx'. \tag{30}$$

The only approximation is in Eq. (27) where we have not taken into account the term $-\partial_x V^{(1)} \partial_k m_k^{(1)}$ which is of higher order.

4.2. Strong collapse boost mediated by the stable homogeneous background

The quantities $\mathcal{N}^{(1)} = (2\pi)^{-1}\int N^{(1)}(x,z)dx$ and $\mathcal{M}^{(1)} = (2\pi)^{-1}\int M(x,z)dx$ are conserved during the evolution in z. As in the case of the weak background regime discussed in Section 3, the enhancement of the collapse mediated by the background, is not due to a transfer of 'mass' from the background toward the collapsing structure, but a transfer of momentum. To see this, we recall that the momentum $K^{(1)}(x,z)$ is initially driven by the last nonlinear term in (29) and then the Burgers-like term of (29) develops the gradient catastrophe of $K^{(1)}(x,z)$ toward the point located at $x = 0$. As we show below, the presence of the background $m_k^{(0)}$ has an impact on the initial drive of $K^{(1)}(x,z)$.

In the absence of background, the singular component satisfies (28)–(29)–(30) with $M^{(1)} = 0$. In the presence of background, the term $M^{(1)}$ is not zero for positive z. From (27), the mass $M^{(1)}$ satisfies:

$$\partial_z M^{(1)} = -\alpha \partial_x P^{(1)}, \quad P^{(1)} = \int k m_k^{(1)} dk. \tag{31}$$

For small z, we find that $\partial_z m_k^{(1)} + \alpha k \partial_x m_k^{(1)} = -\frac{\gamma}{2\pi}\partial_x(U * N_o^{(1)})\partial_k m^{(0)}$, which gives

$$\begin{aligned} m_k^{(1)}(x,z) &= -\frac{\gamma}{2\pi}\int_0^z \partial_x(U * N_o^{(1)})(x - \alpha k z')dz' \partial_k m_k^{(0)} \\ &\simeq -\frac{\gamma z}{2\pi}\partial_x(U * N_o^{(1)})(x)\partial_k m_k^{(0)}. \end{aligned} \tag{32}$$

Recalling that the functions $U * N_o^{(1)}$ vs. x, and $m_k^{(0)}$ vs. k, are bell-shaped, then the function $m_k^{(1)}(x,z)$ gets square-shaped in phase-space (x,k). The counter-streaming flow with positive velocity (for $k > 0$) and negative velocity (for $k < 0$), then leads to a twist of the square-shaped pattern, as evidenced in Fig. 7(f). Furthermore, substituting (32) into (31), we find $P^{(1)} \simeq \frac{\gamma}{2\pi}\partial_x(U * N_o^{(1)})M^{(0)}z$ and

$$M^{(1)}(x,z) \simeq -\frac{\alpha\gamma M^{(0)} z^2}{4\pi}\partial_x^2(U * N_o^{(1)})(x).$$

This means that the presence of the background changes the initial drive $\partial_x V^{(1)} = -\frac{\gamma}{2\pi}\partial_x(U * \tilde{N}^{(1)})$ in Eq. (29) by modifying $\tilde{N}^{(1)} = N_o^{(1)}$ into $\tilde{N}^{(1)} = N_o^{(1)} - \frac{\alpha\gamma M^{(0)} z^2}{4\pi}\partial_x^2(U * N_o^{(1)})$. Since $\alpha\gamma > 0$, this modification induces an enhancement of the amplitude of the peak $\tilde{N}^{(1)}$ and a reduction of its radius, which in turn implies through (29) a stronger gradient catastrophe and through (28) a stronger collapse singularity.

The numerical simulations confirm this qualitative analysis, as illustrated in Fig. 7. We have solved numerically the set of coupled Eqs. (27)–(30). The enhancement of the collapse instability mediated by the background is evidenced by the sign of $M^{(1)}(x,z) = \int m_k^{(1)}(x,z)dk$, see Fig. 7(c). The background depletes on both sides of the localized beam $M^{(1)}(x,z)$, and the corresponding 'mass' contracts on the collapse structure at $x \simeq 0$, while there is no 'mass' exchange between the background and the collapse structure. The simulation of the Vlasov Eq. (2) also confirms the global behavior, as revealed by the corresponding phase-space evolution, where the local spectrum of the wave-packet exhibits the expected peculiar folding discussed above, see Fig. 7(d). Note that in Fig. 7, the perturbative regime (25)–(26) considered in the theory is well verified during the first stage of propagation ($z \lesssim 90L_{nl}$), while it is not verified nearby the singularity ($z \simeq 90L_{nl}$).

The simulations of the Vlasov equation also evidence the enhancement of the collapse peak mediated by the background. We report in Fig. 7(g) the enhancement of the collapse peak intensity for different background levels $M^{(0)}$. Starting from the same Gaussian intensity profile, we vary the background levels $M^{(0)}$, revealing that the collapse peak increases significantly with the background level.

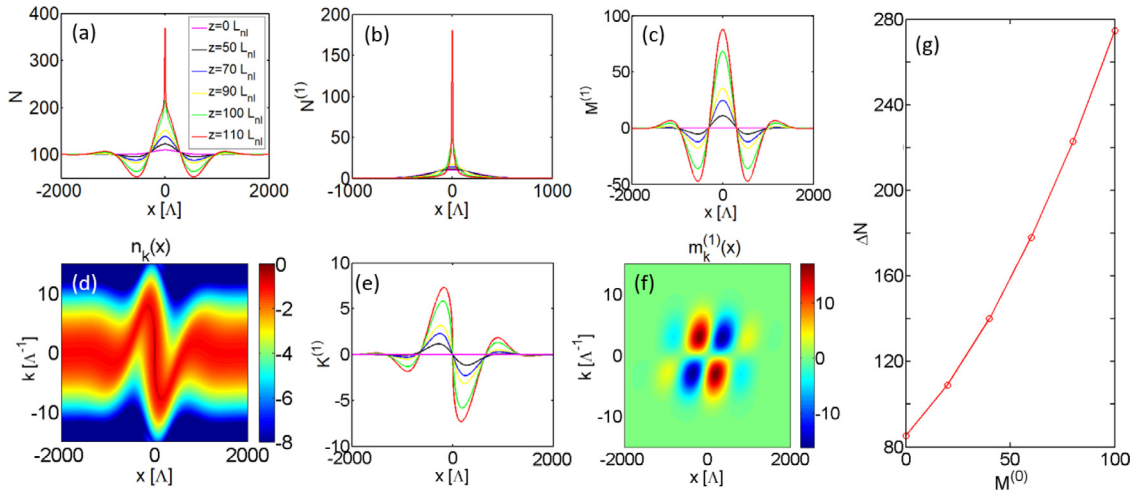

Fig. 7. Collapse boost mediated by a strong background. Numerical simulations of the set of Eqs. (27)–(30). It includes the hydrodynamic model for the singular collapse structure $(N^{(1)}(x,z), K^{(1)}(x,z))$ given in Eqs. (28)–(29), which is coupled to the incoherent background. The incoherent background is composed of the strong constant background $M^{(0)}$, and its small deformation $m_k^{(1)}(x,z)$ governed by the reduced Vlasov Eq. (27). The sum of the intensity contributions $N(x,z) = N^{(1)}(x,z) + M^{(0)} + M^{(1)}(x,z)$ is reported in (a). The different colors report the quantities at different propagation lengths, see the legend in (a). The transfer of momentum $K^{(1)}(x,z)$ between the background and the collapse structure drives the background-enhanced collapse: The sign of $M^{(1)}(x,z) = \int m_k^{(1)}(x,z)dk$ is important and denotes an enhancement ($M^{(1)}(x) > 0$) or a decrease ($M^{(1)}(x) < 0$) of the collapsing structure due to the presence of the stable background: The 'mass' on both sides of the localized beam $M^{(1)}(x,z)$ is transferred toward the beam center, which leads to an enhancement of the collapse structure at $x \simeq 0$. We recall that there is no 'mass' exchange between the background and the collapse structure, $\int M^{(1)}(x,z)dx = 0$ for any z. (d) $n_k(x)$ obtained by simulation of the Vlasov Eq. (2), for $z = 110L_{nl}$ ($\log_{10}$-scale). (e) Evolution of the first-order momentum. (f) The square-shaped pattern of $m_k^{(1)}(x)$ can be explained through the early stage analysis of the evolution, see Eq. (32) (linear scale). (g) Simulations of the Vlasov Eq. (2) showing the collapse peak enhancement mediated by the background, $\Delta N = N_{\max} - M^{(0)}$ for different background levels $M^{(0)}$.

5. Discussion and conclusion

5.1. Toward an incoherent rogue wave phenomenon

In summary, by considering the nonlocal NLS equation, we have shown that an incoherent speckle beam that evolves in the strongly nonlinear and highly nonlocal regime exhibits a collective incoherent collapse, which is characterized by a significant reduction of the coherence length at the beam center while the peak of the incoherent beam envelope increases dramatically. We have shown that the presence of a homogeneous incoherent background favors the development of the incoherent collapse, in spite of the fact that the background is modulationally stable. The theoretical analysis is based on the wave-turbulence Vlasov equation. By looking for solutions to the Vlasov equation in the form of singular components coupled to smooth components, we have shown that the collapse dynamics is governed by a hydrodynamic model coupled to the incoherent background by an effective Vlasov equation. In this way, we have treated the weak and strong background regimes, and we have shown that the strong incoherent background significantly boosts the collapse instability.

We briefly comment here the possible applicability of our study to extreme wave events, e.g., rogue, or freak waves [18, 111]. Although extreme wave amplitudes have been shown to emerge from a turbulent state, so far, the rogue wave itself has been always considered as being inherently a *coherent localized entity*. Here, we have shown that a weak intensity perturbation with a coherence higher than that of the underlying incoherent background, can lead to the formation of a high-amplitude incoherent event, a feature that may be interpreted in analogy with an incoherent rogue wave phenomenon. Indeed, as discussed above, the 'mass' of the background tends to concentrate on the singular collapse: The depletion of the background on both sides of the collapse structure strengthens the growth of the collapse instability. It turns out that the intensity profile of the giant collapse peak observed in Fig. 7(a) exhibits some resemblance with a 'breather' structure [111–122], which is known as a prototype for an extreme event featured by a spatiotemporal localization of a coherent pulse over a constant-finite background. In future investigations we plan to study the spontaneous emergence and the statistics of the incoherent collapse events revealed in this work.

5.2. Theoretical description of the 2D incoherent collapse

The theory of the incoherent collapse phenomenon discussed above has been restricted to 1D spatial systems. Here we extend the theory to 2D, which is particularly relevant to nonlinear optics experiments, see Section 5.2.2. The main result is that the incoherent collapse occurs more efficiently in 2D systems as compared to 1D systems.

Exploiting the property of radial symmetry and strong nonlinear interaction, it was shown in Ref. [68] that the 2D Vlasov Eq. (2) can be reduced to an effective 1D radial Vlasov equation:

$$\partial_z \check{n}_k(r,z) + \beta k \partial_r \check{n}_k(r,z) - \partial_r V \partial_k \check{n}_k(r,z) = 0, \tag{33}$$

where $\check{n}_k(r,z) = kr\, n_k(r,z)$, with $r = |\boldsymbol{r}|$ and $k = |\boldsymbol{k}|$. We have

$$V(r,z) = -\frac{\gamma}{(2\pi)^2} \int_0^\infty \tilde{U}(r,r')\check{N}(r',z)dr', \tag{34}$$

$$\tilde{U}(r,r') = \int_0^{2\pi} U\left(\sqrt{r^2 + r'^2 - 2rr'\cos\theta}\right)d\theta, \tag{35}$$

$$\check{N}(r,z) = \int_0^\infty \check{n}_k(r,z)dk = rN(r,z). \tag{36}$$

Following the procedure discussed above in 1D, we study the collapse behavior through the analysis of singular solutions of the effective Vlasov Eq. (33):

$$\check{n}_k(r,z) = \check{N}(r,z)\delta\big(k - K(r,z)\big), \tag{37}$$

where the 'density' $\check{N}(r,z)$ and 'momentum' $K(r,z)$ satisfy the hydrodynamic-like equations

$$\partial_z \check{N} + \alpha \partial_r(\check{N}K) = 0, \tag{38}$$

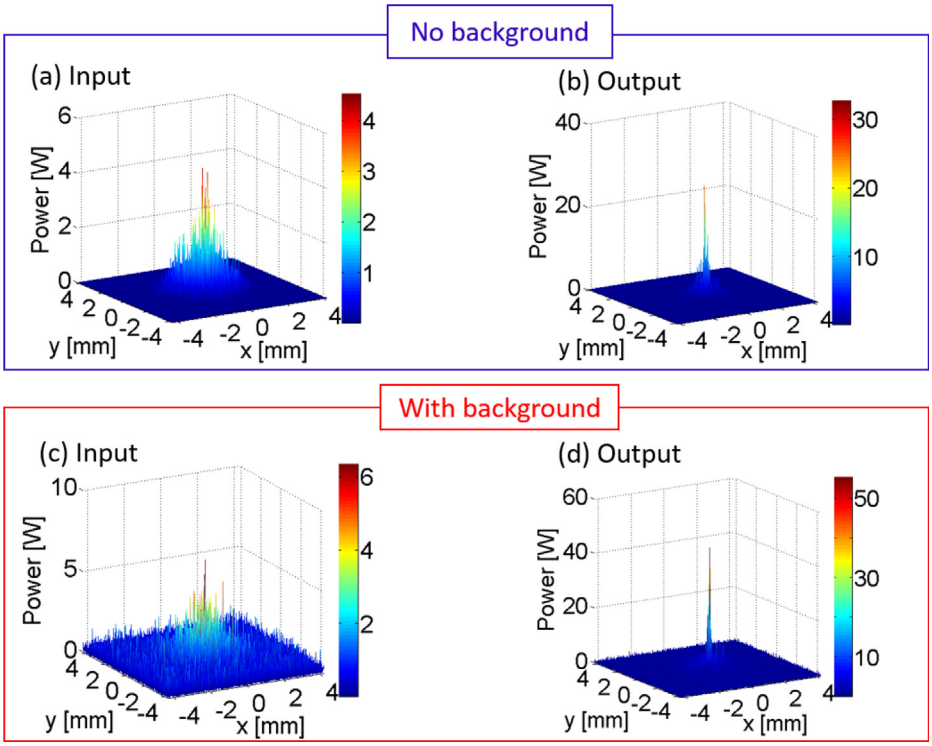

Fig. 8. Collapse dynamics with a thermal nonlinear optical response. Numerical simulations of the 2D NLS Eq. (1) realized with the thermal nonlinear optical response $U(r)$ given in Eq. (52) that is relevant to nonlinear optics experiments in lead glasses. The simulation has been realized with parameters that are accessible to currently available experiments, see the text for details on experimental parameters. Injected speckle beam without background (a), and corresponding collapse peak formed at the output of the sample (b). (c) Same injected speckle beam as in (a), but superimposed on a (modulationally stable) incoherent background, and corresponding collapse peak formed at the output of the sample (d).

$$\partial_z K + \alpha K \partial_r K + \partial_r V = 0. \tag{39}$$

We follow the 1D procedure, and solve these hyperbolic equations by the method of characteristics. Defining the quantities $w(z) = K(R(z),z)$, $\tau(z) = \partial_z K\big(R(z),z\big)$, $\xi(z) = \partial_r K\big(R(z),z\big)$, $\phi(z) = \check{N}\big(R(z),z\big) = R(z)N\big(R(z),z\big)$, we obtain

$$\dot{R}(z) = \alpha w(z), \tag{40}$$
$$\dot{w}(z) = \tau(z) + \alpha w(z)\xi(z), \tag{41}$$
$$\dot{\tau}(z) = -\partial_{zr}^2 V(R(z),z) - \alpha\xi(z)\tau(z), \tag{42}$$
$$\dot{\xi}(z) = -\partial_r^2 V(R(z),z) - \alpha\xi^2(z), \tag{43}$$
$$\dot{\phi}(z) = -\alpha\xi(z)\phi(z). \tag{44}$$

with the initial conditions $R(0) = r_0$, $w(0) = 0$, $\tau(0) = -\partial_r V(r_0, z=0)$, $\xi(0) = 0$, $\phi(0) = \check{N}(r_0, z=0)$. We now analyze the collapse singularity separately for a smooth response function and a singular response function, this latter being relevant to nonlinear optics experiments.

5.2.1. Smooth nonlinear response

We assume that the nonlinear response function $U(r)$ is smooth and maximal at $r = 0$, such as a Gaussian-shaped response. We consider the case where the initial intensity profile is much narrower than that of the potential, so that we can approximate $V(r,z) \simeq -\gamma\mathcal{N}U(r)$. The analysis is similar to the 1D case, however, caution should be exercised because in 2D we have $N\big(R(z),z\big) = \phi(z)/R(z)$, so that, contrary to 1D, we can no longer choose the characteristic $R(z) = 0$ to study the singularity. We thus consider a characteristic $R(z)$ starting from a small but positive $r_0 > 0$. We obtain the following solutions to the characteristic equations:

$$\xi(z) = -\frac{\kappa}{\sqrt{\alpha}}\tan\big(\sqrt{\alpha}\kappa z\big), \tag{45}$$

$$\tau(z) = \frac{\tau(0)}{\cos\big(\sqrt{\alpha}\kappa z\big)}, \tag{46}$$

$$\phi(z) = \frac{\phi(0)}{\cos\big(\sqrt{\alpha}\kappa z\big)}, \tag{47}$$

with $\phi(0) = \check{N}_0(r_0)$, $\tau(0) = \gamma\mathcal{N}\partial_r U(r_0) < 0$ and $\kappa = \sqrt{\gamma\mathcal{N}|\partial_r^2 U(0)|}$. In deriving these expressions, we consider that $R(z)$ remains smaller than r_0 so that the approximation $-\gamma\mathcal{N}\partial_r^2 U(R(z)) \simeq \kappa^2$ is valid. Therefore we find

$$w(z) = \tau(0)\frac{\sin\big(\sqrt{\alpha}\kappa z\big)}{\sqrt{\alpha}\kappa}, \tag{48}$$

$$R(z) = r_0 + \tau(0)\frac{1-\cos\big(\sqrt{\alpha}\kappa z\big)}{\kappa^2}. \tag{49}$$

For small r_0 we have $\tau(0) \simeq \gamma\mathcal{N}\partial_r^2 U(0) r_0 + O(r_0^2) = -\kappa^2 r_0 + O(r_0^2)$, so that $R(z) \simeq r_0\cos\big(\sqrt{\alpha}\kappa z\big)$ and we also have $\phi(0) = r_0 N_0(r_0) = r_0 N_0(0) + O(r_0^2)$, so that, by taking the limit $r_0 \to 0$:

$$N(r=0,z) = \lim_{r_0\to 0}\frac{\phi(z)}{R(z)} = \frac{N_0(0)}{\cos^2\big(\sqrt{\alpha}\kappa z\big)}.$$

To summarize, just before the singularity, we have in 2D:

$$\partial_r K(0,z) \simeq \frac{-1}{\alpha(z_\infty - z)}, \tag{50}$$

$$N(0,z) \simeq \frac{N_0(0)}{\alpha\kappa^2(z_\infty - z)^2}. \tag{51}$$

Then the divergence of the gradient of the momentum has the same form as in 1D, see Eq. (15). On the other hand the intensity peak diverges as $\sim z^{-1}$ in 1D (see Eq. (16)), whereas in 2D the divergence is accelerated as $\sim z^{-2}$, which reflects the intuitive idea that the nonlinear contraction of the beam intensity occurs more efficiently in 2D than in 1D.

5.2.2. Thermal (singular) nonlinear response

Our work should stimulate nonlinear optics experiments by considering the propagation of a speckle beam in a focusing thermal nonlinear medium, such as a lead glass. Lead glasses exhibit a highly nonlocal nonlinear response with a focusing nonlinearity and they have been widely used for the observation of spatial optical solitons [61–64]. In lead glasses, the laser beam acts as a heat source in the material. Heat then diffuses in the material yielding a non-uniform temperature distribution and the induced change of the refractive index follows a diffusion heat equation. As a consequence, the normalized nonlinear response in the 2D NLS Eq. (1) takes the form [68,74,78]

$$U(r) = \frac{1}{2\pi\sigma^2} K_0(r/\sigma), \tag{52}$$

where $K_0(x)$ denotes the modified Bessel function of second kind (zero-th order).

To show that the singular response function (52) also leads to a collapse singularity, we analyze the behavior of the potential $\partial_r^2 V(r,z)$ involved in Eq. (43) for the gradient of the momentum $\xi(z)$. We consider again the case where the initial intensity profile is much narrower than that of the potential. Given the log-singularity of U at 0, the behavior of the potential $V(r,z)$ in the neighborhood of $r = 0$ requires special attention. We have $K_0(s) = -(\log s - \ln 2 + \gamma)(1 - s^2/4) - s^2/4 + o(s^2)$ for small s so that

$$\begin{aligned}\partial_r V(r,z) &= -\frac{\gamma}{(2\pi\sigma)^3}\int_0^\infty\int_0^{2\pi} K_0'(\sqrt{r^2+r'^2-2rr'\cos\theta}) \\ &\quad\times \frac{r - r'\cos\theta}{\sqrt{r^2+r'^2-2rr'\cos\theta}} d\theta \check{N}(r')dr' \\ &\simeq \frac{\gamma}{(2\pi\sigma)^3}\int_0^\infty\int_0^{2\pi} \frac{r - r'\cos\theta}{r^2+r'^2-2rr'\cos\theta} d\theta\check{N}(r')dr',\end{aligned}$$

for small r (i.e., smaller than σ). Since

$$\int_0^{2\pi} \frac{r - r'\cos\theta}{r^2+r'^2-2rr'\cos\theta} d\theta = \frac{2\pi}{r}\mathbf{1}_{[0,r]}(r'),$$

where $\mathbf{1}_{[0,r]}(r') = 1$ for $0 \le r' \le r$ and zero for $r' > r$, we find that

$$\partial_r V(r,z) \simeq \frac{\gamma}{(2\pi)^2\sigma^3 r}\int_0^r \check{N}(r')dr',$$

for small r (i.e., smaller than σ). Using $\check{N}(r) = rN(r)$, we finally find that the second derivative of V has the form

$$\partial_r^2 V(r,z) \simeq \frac{\gamma}{(2\pi)^2\sigma^3}\Big(N(r) - \frac{1}{r^2}\int_0^r r'N(r')dr'\Big),$$

for small r (i.e., smaller than σ), and it is equal to $\frac{\gamma N(0)}{2(2\pi)^2\sigma^3}$ at the center $r = 0$. Since this is positive, then Eq. (43) can be bounded as $\dot{\xi}(z) \le -\alpha\xi^2$, and thus $\xi(z)$ blows up in finite 'time'. Furthermore, we have $\phi(z) \sim \exp(-\alpha\int_0^z \xi(s)ds)$ from Eq. (44), and the envelope intensity of the incoherent beam also blows up in finite 'time'. Then the dynamics described in the case of a smooth response function in Section 5.2.1 can be observed with the singular potential in Eq. (52).

We have confirmed this conclusion by performing numerical simulations of the NLS equation by considering a thermal nonlinearity. Our aim here is to confirm that a thermal nonlinearity with a response function $U(r)$ of the form given by Eq. (52) provides a collapse singular behavior similar to that discussed above for a smooth response function. We have performed simulations of the NLS Eq. (1) with parameters that should be accessible to currently available experiments realized in lead glasses. In the simulation reported in Fig. 8, we consider a laser (wavelength 0.5 μm) that passes through a diffuser to generate a speckle beam of $\simeq$ 2.9 mm (FWHM), with correlation length $\lambda_c^0 \simeq 80$ μm, and average power $\simeq$ 1.85 W, which is injected in a lead glass sample of length $\simeq$12.6 cm. With these parameters the healing length is $\Lambda \simeq 4.26$ μm. As discussed in detail in Ref. [78], the nonlocal length involved in Eq. (52) is essentially determined by the boundary conditions imposed by the lead glass sample [78]. We have considered in Fig. 8 a value of $\sigma \simeq 3.4$ mm that is compatible with typical lead glass samples considered in Refs. [62,78]. In this way, we verify the required separation of spatial length scales $\sigma \gg \lambda_c^0 \gg \Lambda$. The simulations reported in Fig. 8(a)–(b) confirm that the speckle beam exhibits a collapse instability. Furthermore, Fig. 8(c)–(d) also confirms that the development of such a collapse is favored by the presence of a homogeneous incoherent background — we have considered a correlation length $\simeq 4$ μm in Fig. 8(c)–(d).

CRediT authorship contribution statement

Gang Xu, Adrien Fusaro, Antonio Picozzi: Numerical simulations; **Josselin Garnier**: Theoretical developments; **Antonio Picozzi, Gang Xu, Josselin Garnier**: Supervision of the work and manuscript writing.

Declaration of competing interest

The authors declare that they have no known competing financial interests or personal relationships that could have appeared to influence the work reported in this paper.

Acknowledgments

We acknowledge financial support from the Centre national de la recherche scientifique (CNRS), Conseil régional de Bourgogne Franche-Comté, iXCore Research Fondation, Agence Nationale de la Recherche (ANR-19-CE46-0007, ANR-15-IDEX-0003, ANR-21-ESRE-0040), H2020 Marie Sklodowska-Curie Actions (MSCA-COFUND) (MULTIPLY Project No. 713694). Calculations were performed using HPC resources from DNUM CCUB (Centre de Calcul, Université de Bourgogne).

References

[1] V.E. Zakharov, V.S. L'Vov, G. Falkovich, Kolmogorov Spectra of Turbulence I, Springer, Berlin, 1992.
[2] S. Dyachenko, A.C. Newell, A. Pushkarev, V.E. Zakharov, Optical turbulence: weak turbulence, condensates and collapsing filaments in the nonlinear Schrödinger equation, Physica D 57 (1992) 96.
[3] A.C. Newell, S. Nazarenko, L. Biven, Wave turbulence and intermittency, Physica D 152 (2001) 520.
[4] V. Zakharov, F. Dias, A. Pushkarev, One-dimensional wave turbulence, Phys. Rep. 398 (2004) 1–65.
[5] S. Nazarenko, Wave Turbulence, in: Lectures Notes in Physics, Springer, 2011.
[6] A.C. Newell, B. Rumpf, Wave turbulence, Annu. Rev. Fluid Mech. 43 (2011) 59–78.
[7] J. Laurie, U. Bortolozzo, S. Nazarenko, S. Residori, One-dimensional optical wave turbulence: Experiment and theory, Phys. Rep. 514 (2012) 121–175.
[8] A. Picozzi, J. Garnier, T. Hansson, P. Suret, S. Randoux, G. Millot, D. Christodoulides, Optical wave turbulence: Toward a unified nonequilibrium thermodynamic formulation of statistical nonlinear optics, Phys. Rep. 542 (2014) 1–132.
[9] S. Galtier, S.V. Nazarenko, Turbulence of weak gravitational waves in the early universe, Phys. Rev. Lett. 119 (2017) 221101.
[10] S. Galtier, S.V. Nazarenko, Direct evidence of a dual cascade in gravitational wave turbulence, Phys. Rev. Lett. 127 (2021) 131101.
[11] V.S. L'vov, Y. L'vov, A.C. Newell, V. Zakharov, Statistical description of acoustic turbulence, Phys. Rev. E 56 (1997) 405.

[12] A.C. Newell, B. Rumpf, V.E. Zakharov, Spontaneous breaking of the spatial homogeneity symmetry in wave turbulence, Phys. Rev. Lett. 108 (2012) 194502.
[13] E. Turitsyna, G. Falkovich, A. El-Taher, X. Shu, P. Harper, S. Turitsyn, Optical turbulence and spectral condensate in long fibre lasers, Proc. R. Soc. Lond. Ser. A 468 (2012) 2145.
[14] E. Turitsyna, S. Smirnov, S. Sugavanam, N. Tarasov, X. Shu, S. Babin, E. Podivilov, D. Churkin, G. Falkovich, S. Turitsyn, The laminar-turbulent transition in a fibre laser, Nat. Photon. 7 (2013) 783.
[15] D.V. Churkin, I.V. Kolokolov, E.V. Podivilov, I.D. Vatnik, S.S. Vergeles, I.S. Terekhov, V.V. Lebedev, G. Falkovich, M.A. Nikulin, S.A. Babin, S.K. Turitsyn, Wave kinetics of a random fibre laser, Nature Commun. 6 (2015) 6214.
[16] M. Conforti, A. Mussot, J. Fatome, A. Picozzi, S. Pitois, C. Finot, M. Haelterman, B. Kibler, C. Michel, G. Millot, Turbulent dynamics of an incoherently pumped passive optical fiber cavity: Quasisolitons, dispersive waves, and extreme events, Phys. Rev. A 91 (2015) 023823.
[17] A.C. White, B.P. Anderson, V.S. Bagnato, Vortices and turbulence in trapped atomic condensates, Proc. Natl. Acad. Sci. USA 111 (2014) 4719–4726.
[18] M. Onorato, S. Residori, U. Bortolozzo, A. Montina, F.T. Arecchi, Rogue waves and their generating mechanisms in different physical contexts, Phys. Rep. 528 (2013) 47–89.
[19] V.E. Zakharov, S.V. Nazarenko, Dynamics of the Bose–Einstein condensation, Physica D 201 (2005) 203.
[20] C. Connaughton, C. Josserand, A. Picozzi, Y. Pomeau, S. Rica, Condensation of classical nonlinear waves, Phys. Rev. Lett. 95 (2005) 263901.
[21] S. Nazarenko, M. Onorato, Wave turbulence and vortices in Bose–Einstein condensation, Physica D 219 (2006) 1.
[22] G. Krstulovic, M. Brachet, Dispersive Bottleneck delaying thermalization of turbulent Bose–Einstein condensates, Phys. Rev. Lett. 106 (2011) 115303.
[23] S. Nazarenko, M. Onorato, D. Proment, Bose–Einstein condensation and Berezinskii-Kosterlitz–Thouless transition in the two-dimensional nonlinear Schrödinger model, Phys. Rev. A 90 (2014) 013624.
[24] A. Fusaro, J. Garnier, K. Krupa, G. Millot, A. Picozzi, Dramatic acceleration of wave condensation mediated by disorder in multimode fibers, Phys. Rev. Lett. 122 (2019) 123902.
[25] K. Baudin, A. Fusaro, K. Krupa, J. Garnier, S. Rica, G. Millot, A. Picozzi, Classical Rayleigh-jeans condensation of light waves: Observation and thermodynamic characterization, Phys. Rev. Lett. 125 (2020) 244101.
[26] B. Rumpf, A.C. Newell, Coherent structures and entropy in constrained, modulationally unstable, nonintegrable, systems, Phys. Rev. Lett. 87 (2001) 054102.
[27] B. Rumpf, A.C. Newell, V.E. Zakharov, Turbulent transfer of energy by radiating pulses, Phys. Rev. Lett. 103 (2009) 074502.
[28] C. Josserand, Y. Pomeau, S. Rica, Finite-time localized singularities as a mechanism for turbulent dissipation, Phys. Rev. Fluids 5 (2020) 054607.
[29] L. Bergé, Wave collapse in physics: principles and applications to light and plasma waves, Phys. Rep. 303 (1998) 259.
[30] Y.S. Kivshar, D.E. Pelinovsky, Self-focusing and transverse instabilities of solitary waves, Phys. Rep. 331 (2000) 117.
[31] C. Sulem, P. Sulem, The Nonlinear Schrödinger Equation, Self-Focusing and Wave Collapse, Springer, 1999.
[32] G. Fibich, The Nonlinear Schrödinger Equation, Singular Solutions and Optical Collapse, Springer, 2015.
[33] V.E. Zakharov, Collapse of langmuir waves, Sov. Phys.—JETP 35 (1972) 908.
[34] N. Kosmatov, V. Zakharov, V. Shvets, Computer simulation of wave collapses in the nonlinear Schrödinger equation, Physica D. 52 (1991) 16.
[35] A. Wong, P. Cheung, Three-dimensional self-collapse of langmuir waves, Phys. Rev. Lett. 52 (1984) 1222.
[36] C. Sackett, J. Gerton, M. Welling, R. Hulet, Measurements of collective collapse in a Bose–Einstein condensate with attractive interactions, Phys. Rev. Lett. 82 (1999) 876.
[37] H. Sakaguchi, B.A. Malomed, Suppression of the quantum-mechanical collapse by repulsive interactions in a quantum gas, Phys. Rev. A 83 (2011) 013607.
[38] P. Banerjee, A. Korpel, K. Lonngren, Self-refraction of nonlinear capillary–gravity waves, Phys. Fluids 26 (1983) 2393.
[39] Y. Kivshar, G. Agrawal, Optical Solitons: From Fibers to Photonic Crystals, Academic Press, 2003.
[40] A.L. Gaeta, Catastrophic collapse of ultrashort pulses, Phys. Rev. Lett. 84 (2000) 3582.
[41] R.W. Boyd, S. Lukishova, Y.R. Shen, Self Focusing: Past and Present, in: Topics in Applied Physics, vol. 114, Springer, New York, 2009.
[42] S.L. Shapiro, S.A. Teukolsky, Black Holes, White Dwarfs and Neutron Stars - the Physics of Compact Objects, John Wiley and Sons, New York, 1983.
[43] S. Skupin, M. Saffman, W. Królikowski, Nonlocal stabilization of nonlinear beams in a self-focusing atomic vapor, Phys. Rev. Lett. 98 (2007) 263902.
[44] Y. Linzon, K.A. Rutkowska, B.A. Malomed, R. Morandotti, Magneto-optical control of light collapse in bulk Kerr media, Phys. Rev. Lett. 103 (2009) 053902.
[45] A.S. Desyatnikov, D. Buccoliero, M.R. Dennis, Y.S. Kivshar, Suppression of collapse for spiralling elliptic solitons, Phys. Rev. Lett. 104 (2010) 053902.
[46] B. Shim, S.E. Schrauth, A.L. Gaeta, M. Klein, G. Fibich, Loss of phase of collapsing beams, Phys. Rev. Lett. 108 (2012) 043902.
[47] M.D. Feit, J.A. Fleck, Beam nonparaxiality, filament formation, and beam breakup in the self-focusing of optical beams, J. Opt. Soc. Amer. B 5 (1988) 623.
[48] G.A. Pasmanik, Self-interaction of incoherent light beams, Zh. Eksp. Teor. Fiz. 66 (1974) 490; Sov. Phys. JETP 39 (1974) 234.
[49] V.A. Aleshkevich, S.S. Lebedev, A.N. Matveev, Self-interaction of a noncoherent light beam, Sov. J. Quantum Electron. 11 (1981) 647.
[50] O. Bang, D. Edmundson, W. Królikowski, Collapse of incoherent light beams in inertial Bulk Kerr media, Phys. Rev. Lett. 83 (1999) 5479.
[51] S. Turitsyn, Spatial dispersion of nonlinearity and stability of multidimensional solitons, Theor. Math. Phys. 64 (1985) 226.
[52] O. Bang, W. Krolikowski, J. Wyller, J.J. Rasmussen, Collapse arrest and soliton stabilization in nonlocal nonlinear media, Phys. Rev. E 66 (2002) 046619.
[53] F. Ye, B.A. Malomed, Y. He, B. Hu, Collapse suppression and stabilization of dipole solitons in two-dimensional media with anisotropic semilocal nonlinearity, Phys. Rev. A 81 (2010) 043816.
[54] M. Baranov, Theoretical progress in many-body physics with ultracold dipolar gases, Phys. Rep. 464 (2008) 71.
[55] P. Azam, A. Fusaro, Q. Fontaine, J. Garnier, A. Bramati, A. Picozzi, R. Kaiser, Q. Glorieux, T. Bienaimé, Dissipation-enhanced collapse singularity of a nonlocal fluid of light in a hot atomic vapor, Phys. Rev. A 104 (2021) 013515.
[56] W. Krolikowski, O. Bang, J.J. Rasmussen, J. Wyller, Modulational instability in nonlocal nonlinear Kerr media, Phys. Rev. E 64 (2001) 016612.
[57] W. Krolikowski, O. Bang, N.I. Nikolov, D. Neshev, J. Wyller, J.J. Rasmussen, D. Edmundson, Modulational instability, solitons and beam propagation in spatially nonlocal nonlinear media, J. Opt. B: Quant. Semicl. Opt. 6 (2004) S288.
[58] M. Peccianti, C. Conti, G. Assanto, A. De Luca, C. Umeton, Routing of anisotropic spatial solitons and modulational instability in liquid crystals, Nature 432 (2004) 733–737.
[59] C. Conti, M. Peccianti, G. Assanto, Observation of optical spatial solitons in a highly nonlocal medium, Phys. Rev. Lett. 92 (2004) 113902.
[60] M. Peccianti, G. Assanto, Nematicons, Phys. Rep. 516 (2012) 147.
[61] B. Alfassi, C. Rotschild, O. Manela, M. Segev, D. Christodoulides, Boundary force effects exerted on solitons in highly nonlinear media, Opt. Lett. 32 (2007) 154.
[62] C. Rotschild, O. Cohen, O. Manela, M. Segev, T. Carmon, Solitons in nonlinear media with an infinite range of nonlocality: First observation of coherent elliptic solitons and of vortex-ring solitons, Phys. Rev. Lett. 95 (2015) 213904.
[63] Q. Shou, M. Wu, Q. Guo, Large phase shift of (1+1)-dimensional nonlocal spatial solitons in lead glass, Opt. Commun. 338 (2014) 133.
[64] C. Rotschild, B. Alfassi, O. Manela, M. Segev, Long-range interactions between optical solitons, Nat. Phys. 2 (2006) 769.
[65] N. Ghofraniha, C. Conti, G. Ruocco, S. Trillo, Shocks in nonlocal media, Phys. Rev. Lett. 99 (2007) 043903.
[66] C. Conti, A. Fratalocchi, M. Peccianti, G. Ruocco, S. Trillo, Observation of a gradient catastrophe generating solitons, Phys. Rev. Lett. 102 (2009) 083902.
[67] N. Ghofraniha, L.S. Amato, V. Folli, S. Trillo, E. DelRe, C. Conti, Measurement of scaling laws for shock waves in thermal nonlocal media, Opt. Lett. 37 (2012) 2325.
[68] G. Xu, D. Vocke, D. Faccio, J. Garnier, T. Roger, S. Trillo, A. Picozzi, From coherent shocklets to giant collective incoherent shock waves in nonlocal turbulent flows, Nature Commun. 18 (2015) 947.
[69] M. Karpov, T. Congy, Y. Sivan, V. Fleurov, N. Pavloff, S. Bar-Ad, Spontaneously formed autofocusing caustics in a confined self-defocusing medium, Optica 2 (2015) 1053.
[70] D. Vocke, T. Roger, F. Marino, E.M. Wright, I. Carusotto, M. Clerici, D. Faccio, Experimental characterization of nonlocal photon fluids, Optica 2 (2015) 484.
[71] M.C. Braidotti, S. Gentilini, C. Conti, Gamow vectors explain the shock profile, Opt. Express 24 (2016) 21963.
[72] G.A. El, N.F. Smyth, Radiating dispersive shock waves in non-local optical media, Proc. R. Soc. Lond. Ser. A Math. Phys. Eng. Sci. 472 (2016) 20150633.
[73] D. Vocke, K. Wilson, F. Marino, I. Carusotto, E.M. Wright, T. Roger, B.P. Anderson, P. Öhberg, D. Faccio, Role of geometry in the superfluid flow of nonlocal photon fluids, Phys. Rev. A 94 (2016) 013849.
[74] G. Marcucci, D. Pierangeli, S. Gentilini, N. Ghofraniha, Z. Chen, C. Conti, Optical spatial shock waves in nonlocal nonlinear media, Adv. Phys. X 4 (2019) 1662733.

[75] G. Marcucci, X. Hu, P. Cala, W. Man, D. Pierangeli, C. Conti, Z. Chen, Anisotropic optical shock waves in isotropic media with giant nonlocal nonlinearity, Phys. Rev. Lett. 125 (2020) 243902.
[76] V. Zakharov, S. Musher, A. Rubenchik, Hamiltonian approach to the description of non-linear plasma phenomena, Phys. Rep. 129 (1985) 285.
[77] R. Bekenstein, R. Schley, M. Mutzafi, C. Rotschild, M. Segev, Optical simulations of gravitational effects in the Newton-Schrödinger system, Nat. Phys. 11 (2015) 872–878.
[78] T. Roger, C. Maitland, K. Wilson, N. Westerberg, D. Vocke, E.M. Wright, D. Faccio, Optical analogues of the Newton-Schrödinger equation and boson star evolution, Nat. Commun. 7 (2016) 13492.
[79] F. Marino, Massive phonons and gravitational dynamics in a photon-fluid model, Phys. Rev. A 100 (2019) 063825.
[80] J. Skipp, V. L'vov, S. Nazarenko, Wave turbulence in self-gravitating Bose gases and nonlocal nonlinear optics, Phys. Rev. A 102 (2020) 043318.
[81] A. Paredes, D.N. Olivieri, H. Michinel, From optics to dark matter: A review on nonlinear Schrödinger-Poisson systems, Physica D 403 (2020) 132301.
[82] J. Garnier, K. Baudin, A. Fusaro, A. Picozzi, Coherent soliton states hidden in phase-space and stabilized by gravitational incoherent halos, Phys. Rev. Lett. 127 (2021) 014101.
[83] J. Garnier, K. Baudin, A. Fusaro, A. Picozzi, Incoherent localized structures and hidden coherent solitons from the gravitational instability of the Schrödinger-Poisson equation, Phys. Rev. E 104 (2021) 054205.
[84] G. Biondini, G.A. El, M.A. Hoefer, P.D. Miller, Dispersive hydrodynamics, Physica D 333 (2016) 1.
[85] M. Onorato, S. Resitori, F. Baronio, in: M. Onorato, S. Resitori, F. Baronio (Eds.), Rogue and Shock Waves in Nonlinear Dispersive Media, in: Lecture Notes in Physics, vol. 926, Springer International Publishing, 2016.
[86] G.A. El, M.A. Hoefer, Dispersive shock waves and modulation theory, Physica D 333 (2016) 11.
[87] P.D. Miller, On the generation of dispersive shock waves, Physica D 333 (2016) 66.
[88] L. Romagnani, S.V. Bulanov, M. Borghesi, P. Audebert, J.C. Gauthier, K. Löwenbrück, A.J. Mackinnon, P. Patel, G. Pretzler, T. Toncian, O. Willi, Observation of collisionless shocks in laser-plasma experiments, Phys. Rev. Lett. 101 (2008) 025004.
[89] M.A. Hoefer, M.J. Ablowitz, I. Coddington, E.A. Cornell, P. Engels, V. Schweikhard, Dispersive and classical shock waves in Bose–Einstein condensates and gas dynamics, Phys. Rev. A 74 (2006) 023623.
[90] W. Wan, S. Jia, J.W. Fleischer, Dispersive superfluid-like shock waves in nonlinear optics, Nat. Phys. 3 (2007) 46.
[91] S.K. Ivanov, J.-E. Suchorski, A.M. Kamchatnov, M. Isoard, N. Pavloff, Formation of dispersive shock waves in a saturable nonlinear medium, Phys. Rev. E 102 (2020) 032215.
[92] G. Xu, A. Mussot, A. Kudlinski, S. Trillo, F. Copie, M. Conforti, Shock wave generation triggered by a weak background in optical fibers, Opt. Lett. 41 (2016) 2656.
[93] J. Fatome, C. Finot, G. Millot, A. Armaroli, S. Trillo, Observation of optical undular bores in multiple four-wave mixing, Phys. Rev. X 4 (2014) 021022.
[94] S. Trillo, M. Conforti, Handbook of Optical Fibers, Springer, Singapore, 2017, pp. 1–48,
[95] G. Xu, M. Conforti, A. Kudlinski, A. Mussot, S. Trillo, Dispersive dam-break flow of a photon fluid, Phys. Rev. Lett. 118 (2017) 254101.
[96] S. Trillo, J.S. Totero Gongora, A. Fratalocchi, Wave instabilities in the presence of nonvanishing background in nonlinear Schrödinger systems, Sci. Rep. 4 (2014) 7285.
[97] A. Picozzi, J. Garnier, Incoherent soliton turbulence in nonlocal nonlocal nonlinear media, Phys. Rev. Lett. 107 (2011) 233901.
[98] G. Xu, J. Garnier, D. Faccio, S. Trillo, A. Picozzi, Incoherent shock waves in long-range optical turbulence, Physica D 333 (2016) 310.
[99] M. Segev, D. Christodoulides, Incoherent solitons, in: S. Trillo, W. Torruellas (Eds.), Spatial Solitons, Springer, Berlin, 2001.
[100] V.S. Lvov, A.M. Rubenchik, Spatially non-uniform singular weak turbulence spectra, Sov. Phys.—JETP 45 (1977) 67.
[101] V.E. Zakharov, S.L. Musher, A.M. Rubenchik, Hamiltonian approach to the description of non-linear plasma phenomena, Phys. Rep. 129 (1985) 285–366.
[102] A. Campa, T. Dauxois, D. Fanelli, S. Ruffo, Physics of Long-Range Interacting Systems, Oxford Univ. Press, 2014.
[103] C. Michel, B. Kibler, J. Garnier, A. Picozzi, Temporal incoherent solitons supported by a defocusing nonlinearity with anomalous dispersion, Phys. Rev. A 86 (2012) R041801.
[104] G. Xu, A. Fusaro, J. Garnier, A. Picozzi, Incoherent shock and collapse singularities in non-instantaneous nonlinear media, Appl. Sci. 8 (2018) 2559.
[105] R. Balescu, Equilibrium and Nonequilibrium Statistical Mechanics, Wiley, 1975.
[106] A. Vedenov, L. Rudakov, Interaction of waves in continuous media, Sov. Phys. Dokl. 9 (1965) 1073.
[107] M. Soljacic, M. Segev, T. Coskun, D. Christodoulides, A. Vishwanath, Modulation instability of incoherent beams in noninstantaneous nonlinear media, Phys. Rev. Lett. 84 (2000) 467.
[108] D. Kip, M. Soljacic, M. Segev, E. Eugenieva, D.N. Christodoulides, Modulation instability and pattern formation in spatially incoherent light beams, Science 290 (2000) 495–498.
[109] B. Hall, M. Lisak, D. Anderson, R. Fedele, V.E. Semenov, Statistical theory for incoherent light propagation in nonlinear media, Phys. Rev. E 65 (2002) 035602.
[110] L.C. Evans, Partial Differential Equations, AMS, Providence, 2002.
[111] J. Dudley, F. Dias, M. Erkintalo, G. Genty, Instability, breathers and rogue waves in optics, Nat. Photon. 8 (2014) 755.
[112] E.A. Kuznetsov, Solitons in a parametrically unstable plasma, Sov. Phys. Dokl. 22 (1977) 507–508.
[113] Y.C. Ma, The perturbed plane-wave solutions of the cubic Schrödinger equation, Stud. Appl. Math. 60 (1979) 43.
[114] N. Akhmediev, V.M. Eleonskii, N.E. Kulagin, Exact first-order solutions of the nonlinear Schrödinger equation, Theoret. Math. Phys. 72 (1987) 809–818.
[115] B. Kibler, J. Fatome, C. Finot, G. Millot, F. Dias, G. Genty, N. Akhmediev, J.M. Dudley, The peregrine soliton in nonlinear fibre optics, Nat. Phys. 6 (2010) 790.
[116] M. Erkintalo, K. Hammani, B. Kibler, C. Finot, N. Akhmediev, J.M. Dudley, G. Genty, Higher-order modulation instability in nonlinear fiber optics, Phys. Rev. Lett. 107 (2011) 253901.
[117] S. Toenger, T. Godin, C. Billet, F. Dias, M. Erkintalo, G. Genty, J.M. Dudley, Emergent rogue wave structures and statistics in spontaneous modulation instability, Sci. Rep. 5 (2015) 10380.
[118] A. Chabchoub, N.P. Hoffmann, N. Akhmediev, Rogue wave observation in a water wave tank, Phys. Rev. Lett. 106 (2011) 204502.
[119] A. Chabchoub, N. Hoffmann, M. Onorato, N. Akhmediev, Super rogue waves: Observation of a higher-order breather in water waves, Phys. Rev. X 2 (2012) 011015.
[120] V.E. Zakharov, A.A. Gelash, Nonlinear stage of modulation instability, Phys. Rev. Lett. 111 (2013) 054101.
[121] B. Kibler, A. Chabchoub, A. Gelash, N. Akhmediev, V.E. Zakharov, Superregular breathers in optics and hydrodynamics: Omnipresent modulation instability beyond simple periodicity, Phys. Rev. X 5 (2015) 041026.
[122] G. Xu, A. Gelash, A. Chabchoub, V. Zakharov, B. Kibler, Breather wave molecules, Phys. Rev. Lett. 122 (2019) 084101.